RONNY EICHLER

MULTI-SITE OPTOGENETIC CONTROL OF LOCALIZED NEURONAL CIRCUITS

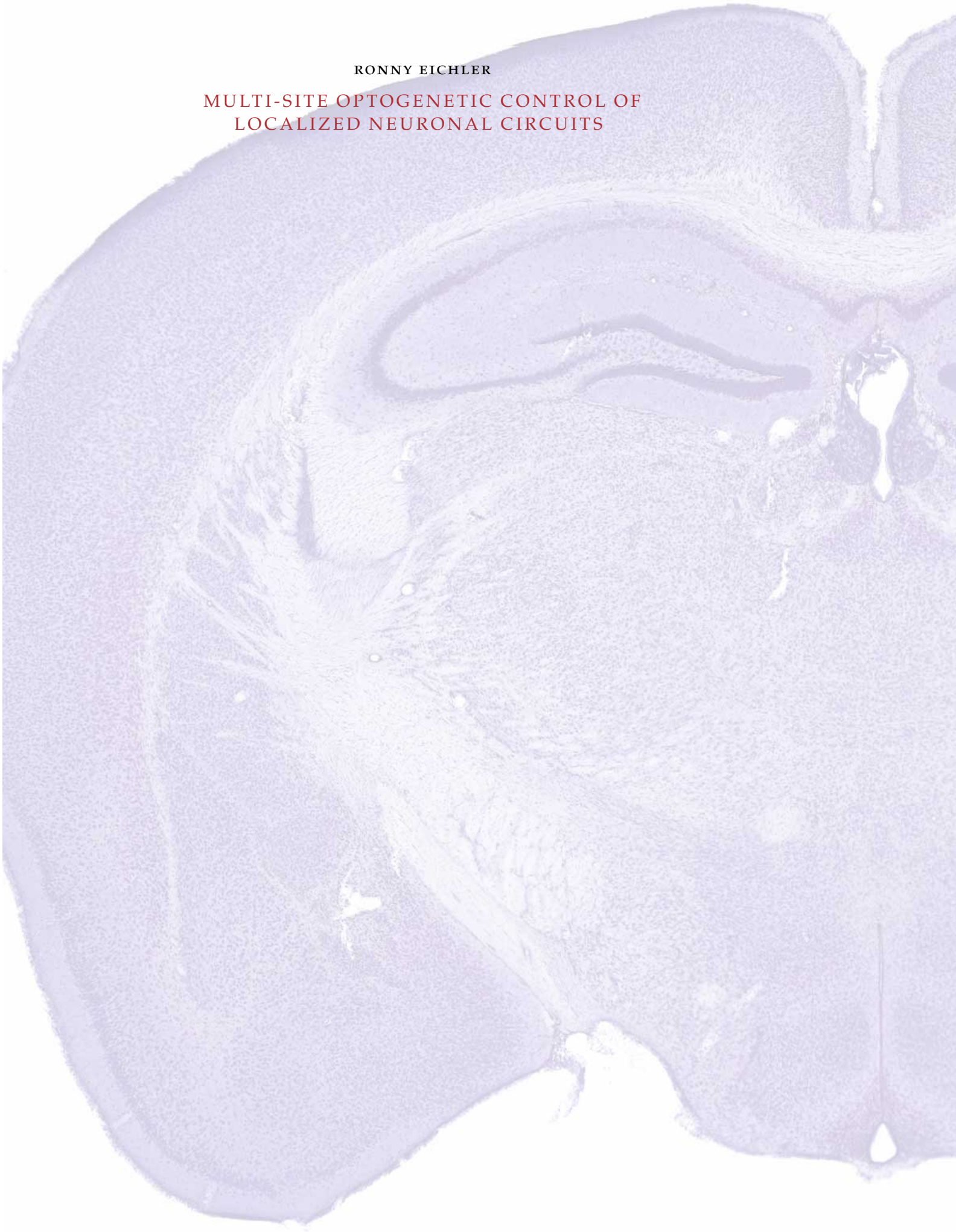

MULTI-SITE OPTOGENETIC CONTROL *of* LOCALIZED NEURONAL CIRCUITS

RONNY EICHLER

July 2013

Submitted in partial fulfillment of the requirements
for the degree of Master of Science

to the

Department of Neurobiology
Faculty of Health and Science
University of Eastern Finland

SUPERVISORS:
Eran STARK, MD, PHD
György BUZSÁKI, MD, PHD
Heikki TANILA, MD, PHD

LOCATION:
Kuopio, Finland

TIME FRAME:
July 2013

ABSTRACT

The recent development of optogenetic tools introduced a novel approach for the interrogation of the nervous system. The exploitation of genetically encoded fast acting light-activated microbial opsins allows for cell-type specific control of neuronal excitability with high temporal precision. In combination with established multi-channel extracellular electrophysiology both observation and perturbation can be achieved simultaneously. However, the spatial resolution of stimulation in awake behaving animals is limited by the tethering and weight limitations for required optics imposed by the small size of laboratory rodents.

Coupling miniature light-emitting diodes (LEDs) or laser diodes (LDs) to small core optical fibers yielded light sources with high power densities. Their small mass and minimal tethering requirement permits placement of several diode-fiber couplets onto the animals head without compromising the freedom of movement.

Optoelectric arrays were constructed by combining multi-shank silicon probes or multiple tetrodes mounted on movable micro-drives with several diode-coupled fibers. Reduction of the fiber diameter by thinning of the cladding and shaping of pointed tips by etching of the fibers allowed to position the fiber tips close ($< 50\,\mu m$) to the recording electrodes. A custom-built multi-channel current source granted high temporal resolution and precise control over stimulation intensity with arbitrary stimulus waveforms.

Diode-probe or diode-tetrode arrays were implanted into the brains of rats and mice expressing channelrhodopsin-2 (ChR2) in cortical and hippocampal neurons. Stimulation reliably evoked cell-type specific optogenetic activation. A large fraction of isolated units was light modulated. The spatial expanse of activation depended on the stimulus intensity with weak light limiting activation to the illuminated shank.

Thus, diode-probes and diode-tetrodes enable precise and versatile spatiotemporal control of specific types of cells in freely behaving animals expressing exogenous opsins.

PUBLICATIONS

Ideas and figures of have previously appeared in the Stark *et al.* work *"Diode probes for spatiotemporal optical control of multiple neurons in freely moving animals"* published 2012 in the Journal of Neurophysiology [59].

An original idea.
That can't be too hard.
The library must be full of them.

— Stephen Fry [20]

ACKNOWLEDGMENTS

I would like to express my sincerest gratitude to my supervisors for their directions and continued support. I am grateful to Prof. György Buzsáki for the most generous and extended welcome to his group. It has been an inspiring experience to have witnessed such vast knowledge and acuity. I am especially thankful for his support of my graduate career.
My sincerest appreciations go to Dr. Eran Stark for his role as a mentor and friend. His guidance and training will be invaluable if I can retain just a small fraction of the tremendous skill and expertise he shared with me. Eran is to be credited for major elements of the presented work. He developed the diode-probe technology, prepared and recorded animals and performed the data analysis.
I must thank Prof. Heikki Tanila for his patience and support. Heikki has been the starting point of my wondrous journey into neuroscience and continued to play a key role in my training.
I am immeasurably indebted to Prof. Dirk Isbrandt for promoting and patronizing me on this incredible journey. I can only hope to be able to repay his trust and efforts in a timely manner.
I want to give special thanks to Dr. Lisa Roux for being such a fantastic and passionate colleague and good friend. She contributed to preparation, implantation and recording of animals and was responsible for all histological figures.
It has been nothing but a pleasure to be in the company of such a fine selection of characters: Adrien, Andres, Brandon, Dan, Dave, Erik, Gabrielle, Jagdish, John, Kenji, Marie, Shige, Toni... Thanks[1].
For the unexpected length of my visit I greatly depended on the administrative and organizational wizardry of Celina Caban, Reagan Barron and Dr. Heather McKellar, and Carol Roehrenbeck for sharing her home with me during all this time, providing shelter from natural disasters and sunlight alike.
As a most pleasent side-effect of this enterprise, I want to thank Esther Holleman for the outlook of hopefully continued cooperation, collaboration and cohabitation.
The very last words of deepest appreciation go to my family. But I am sure they have grown accustomed to waiting to hear from me.

1 A lot. For indulgences, occasional couches and discussions.

CONTENTS

LIST OF FIGURES

ACRONYMS

7TM	seven transmembrane domain
AAV	adeno-associated virus
AP	action potential
AWG	american wire-gauge
bp	base pairs
CA1	*cornu ammonis* area 1
CA3	*cornu ammonis* area 3
CAG	CMV early enhancer/chicken beta actin promotor
CaMKIIα	Calcium/calmodulin-dependent protein kinase type II alpha chain
CCD	charge-coupled device
ChR2	channelrhodopsin-2
COD	catastrophic optical damage
CoM	center-of-mass
Cx	cortex
D	duty cycle
DAC	digital-analog conversion
DAPI	4′,6-diamidino-2-phenylindole
DC	direct current
DG	dentate gyrus
DIP	dual inline package
DNA	deoxyribonucleic acid
DOF	degrees of freedom
DSP	digital signal processor
DPSS	diode-pumped solid state
eNpHR3.0	enhanced *Natronomonas pharaonis* halorhodopsin 3.0

EYFP	enhanced yellow-fluorescent protein
GPCR	G-protein coupled receptor
Halo	eNpHR3.0
HF	hydrofluoric acid
IC	integrated component
I_f	forward current
IUE	*in-utero* electroporation
INT	putative interneuron
LED	light-emitting diode
LD	laser diode
LFP	local field potential
MEA	multi-electrode array
NA	numerical aperture
NAND	logical not-AND gate
NPN	bipolar junction N-channel transistor
op-amp	operational amplifier
PBS	phosphate buffered saline
PCA	principle component analysis
PCB	printed circuit board
PSTH	peri-stimulus time histogram
PNP	bipolar junction P-channel transistor
PV	Parvalbumin
PYR	putative pyramidal cell
RI	refractive index
SD	standard deviation
SEM	standard error of the mean
SFO	step-function opsin
SMT	surface mount technology
TTL	transistor-transistor logic
UV	ultra-violet

1

INTRODUCTION

Small laboratory animals, foremost rodents like mice and rats, are a crucial platform for behavioral and circuit level neuroscience [68]. They offer a wide range of genetic tools and behavioral paradigms and their anatomy is well documented. However, their body size imposes limitations on recording hardware and tethering for experiments involving the awake freely moving animals [7, 17, 41]. The introduction of optogenetics increased the challenge in designing high-fidelity miniature recording gear with an increasing number of channels, while accommodating concurrent optogenetic stimulation [8, 1].

1.1 OPTOGENETICS

While a large variety of methods for perturbation of excitable cells exists, these traditionally have substantial limitations for interrogation of neural circuits. Electrical and physical methods provide temporal precision but have poor spatial selectivity, while genetic and pharmacological methods have severely limited temporal resolution and are often accompanied by unwanted or unknown side effects [13].

Optogenetics as a very recent addition to the neuroscience toolbox is promising to greatly extend the ability of scientists to interact with neuronal circuitry. The core of optogenetics is the use of genetically encoded light-controlled molecular actuators [8, 14, 69]. The combination of existing genetic and proteomic tools, a large and quickly increasing variety of such actuators (Figure 1, [72, 19]) and the use of photons as the signaling channel combines spatiotemporal precision with cell type specificity [9, 15, 24, 35]. A steadily increasing number of publications has already demonstrated its power and ease of adoption (see review by Tye and Deisseroth [61]).

1.1.1 *Optogenetic actuators*

A wide range of optogenetic probes for different use cases exists (Figure 1, [40]). The most commonly used are engineered versions of natural microbial or mammalian opsins (others include control of protein activity using fluorescent proteins [73]). Opsins are seven transmembrane domain (7TM) proteins which are able to interact with

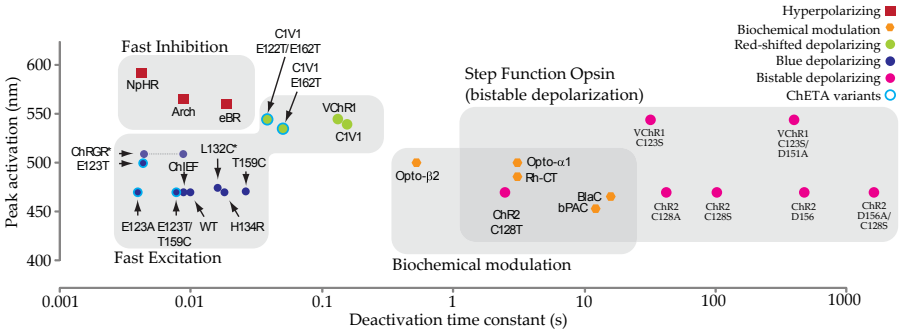

Figure 1: A large variety of opsins available is covering available the spectrum of peak absorption wavelengths and activation kinetics. Most notably fast depolarizing probes like channelrhodopsins (ChR2, VChR1) and the significantly improved mutations, as well as the hyperpolarizing halorhodopsin variants (NpHR) and archaerhodopsin (Arch). See Lin [40] for review; adapted from Yizhar et al. [67]

.

chromophores (retinal or vitamin A) for light sensitivity [52, 14, 50]. Their activation by light pulses typically allows the translation of ions across the membrane, altering the electric potential of the targeted cell [9, 23, 26, 42]. Alternatively chimeric proteins with G-protein coupled receptors (GPCRs) allow the modulation of intracellular signaling [32, 34].

1.1.1.1 *Depolarizing probes*

Depolarizing optogenetic probes shift the membrane potential of affected neurons, greatly increasing the likelihood of action potential (AP) initiation. The most widely used in current *in vivo* research are channelrhodopsins. These non-specific light-gated cation channel are permeable to H^+, Na^+, K^+ and Ca^{2+} ions [49, 5]. Channelrhodopsin-1 (ChR1) and channelrhodopsin-2 (ChR2) are the most prominent examples, expressed by the green algae *Chlamydomonas reinhardtii* as part of its phototaxis cascade [50]. The wild type channelrhodopsin has a peak activation wavelength of 480 nm [4]. A range of engineered versions with shifted peaks exist, allowing to match the opsin to available stimulation optics and the use of multiple optogenetic probes with sufficiently separated spectra [53, 61]. Opsin activating absorbs photons via its chromophore (retinal or vitamin A) [50, 49], causing a conformation change and opening the channel pore and ions can diffuse passively across the membrane. Without light, the chromophore relaxes within milliseconds (Figure 1, [9, 70], quickly closing the pore. These fast activation and deactivation kinetics allow tight temporal control over targeted cells. The maximum stimulation frequency of 40 Hz has been greatly increased with recent engineered variants reaching up to 250 Hz. Most notably the ChR2 mutations ChETA, ChiEF and ChEF, but also mutations with novel kinet-

ics, like step-function opsin (SFO) and stabilized step function opsins [9, 24, 41, 70]. Opsins from other species, like VChR1 from Volvox multicellular algae, can contribute novel characteristics, in this case a red-shifted activation peak of 535 nm allows use of multiple opsins and deeper penetration of activation.

1.1.1.2 *Hyperpolarizing probes*

There are exceptions where the chloride current depolarizes, for example when the chloride reversal is sufficiently shifted.

In contrast to depolarizing probes, hyperpolarizing optogenetic actuators typically inhibit spike initiation of cells, down to completely silencing neurons. At the time of writing, halorhodposin (NpHR), a light-driven Cl^- pump expressed by the halobacterium *Natronomonas pharaonis*, is the most commonly used hyperpolarizing opsin *in vivo* [6, 39, 38, 57]. The activation mechanics are similar to channelrhodopsin with a chromophore (retinal or vitamin A) absorbing photons and activating the probe. The wild type protein has a peak activation with yellow light at around 570 nm. While the conductance is passive for channelrhodopsins, halorhodopsin is a ion pump, actively carrying ions across the membrane [38]. For efficient use in mammalian neurons halorhodopsin was improved by adding and improving trafficking sequences (enhanced halorhodopsin, eNpHR, [22]) and increased photocurrents (eNpHR3.0), improving overall membrane hyperpolarization in response to light [23, 42].

Recently the palette of microbial rhodopsins able to efficiently inhibit neuronal activity has been extended with the discovery of the light-driven proton pump Arch from *Halorubrum sodomense* [15, 23], responding to yellow light, and its stronger homolog ArchT [27]. Mac and eBR, engineered from *Leptosphaeria maculans* [30] and *Halobacterium salinarum* bacteriorhodopsins expand the available spectrum for optogenetic inhibition to blue-green light [15].

1.1.2 *Gene delivery and selective neuron targeting*

Optogenetic probes are genetically encoded with relatively small gene sizes (< 1000 DNA bp) and usually do not require the addition of ligands into the target tissue. This exposes the full range of available genetic methods, from gene delivery, cell type specific expression and control over intracellular trafficking [43]. Existing techniques in molecular biology aide the quick development of advanced versions and the construction of fusion proteins for complex control schemes and precise labeling [40].

The most common method for genetic transfer of optogenetic probes is injection of viral vectors into the volume of interest. Vectors typically consist of replication defective lentiviruses or recombinant adeno-associated viruses [43, 67, 71]. The payload of viruses is very limited however, making it difficult to place the optogenetic transgene under control of a cell type specific promoter, as those are often too large.

Additionally, lentiviruses integrate the genetic material into the host genome where it can interfere with normal function and becomes susceptible to epigenetic silencing [71].

In-utero electroporation (IUE) allows to introduce the transgene at specific time points during the development, allowing for tissue specificity [63, 48] by timing the with the formation of cell layers. IUE however is invasive and can have other risks (e.g. mosaic expression).

For mice (and in a limited number also for rats) a wide range of transgenic strains are available. These allow better control over cell type specific transgene expression.

A major addition to the transgenic toolbox are Cre-recombinase based expression systems [44, 45, 66]. By controlling Cre-expression with the often weak cell-type specific promoter, the transgene itself can be placed under control of a strong ubiquitous promoter and flanked by sites recognized by Cre. In cells expressing Cre even in small quantities, the enzyme will recognize the sites and allow expression of the strongly driven transgene. In addition, this allows to combine viral and non-viral gene delivery methods. The result is a highly modular system for transgene expression. A great example of this modularity is the combination of Cre-driver lines with Cre-reporter lines. For example the PV::Cre and CamKIIa::Cre combined with Ai32 reporter line carrying a ChR2H134R-EYFP construct [44, 45].

1.2 LIGHT DELIVERY

In principle, any light source could be used if the intensity achieved at the target location is higher than the activation threshold for the opsin. But in the real use case each application has further requirements that have to be taken into consideration. Most notably the combination of intended intensity at required and available wavelengths, size and location of the target volume. Furthermore, trade-offs exist between achievable light penetration depth and thermal effects, which can cause tissue damage or alter cell activity and neuronal excitability [33, 68].

1.2.1 *Light sources*

While arc lamps or diode-pumped solid state (DPSS) lasers can be applicable for most applications and deliver high intensities [2, 55, 12], they are impractical for placing light sources close to the area of effect due to size and cooling requirements. Small high efficiency solid state light sources like laser diodes (LDs) and light-emitting diodes (LEDs) on the other hand allow scalable integration at high intensities [33, 59].

LEDs and LDs are electrically behaving like typical semiconductor diodes, however with higher forward voltage (V_f) drops (1 V to 6 V

compared to 0.2 V to 0.5 V for most small-power diodes) primarily depending on the wavelength and material. This forward voltage translates to a high threshold at which the characterizing I/V function dramatically increases in slope. Diodes are highly linear devices over their operating range, especially LEDs emit light in mostly linear dependence to the applied forward current (I_f). In the last decade large progress has been made in extending the variety of available wavelengths, as well as greatly improving the efficiency, the latter which is expressed as Haitz's law [25], predicting an exponential development in the efficiency of LEDs. With Auger recombination identified as the major mechanisms behind current limitations in increasing the light density, this development is likely to continue [31]. High efficiencies translate to low thermal losses and reduced heating at the component level, but also to a luminous flux in small surface areas, lending these light sources to coupling into fibers with small core diameters.

At low currents laser diodes (LDs) operate similar to LEDs. However, their bulk light output is achieved by an electrically pumped laser. Once the applied I_f reaches a threshold, photons in an optical cavity cause an avalanche effect in the pumped medium, emitting a highly coherent and high intensity beam from the facet of the crystal. This lasing threshold complicates the electrical control of LDs, as they have both, a threshold voltage and a threshold current. For most LDs available, these parameters vary between individual components. Additionally, the employed crystals are mechanically fragile and susceptible to heating, being high power devices in small packages. Furthermore the emitting facet can easily be overloaded with photons, as pulses of less than a millisecond duration can cause catastrophic optical damage (COD).

1.2.2 *Drivers and control*

To facilitate independent driving of diodes with common anodes (e.g. multi-color LDs) requires a current source. While diode-based light-sources are partly operating in a linear fashion, their characteristics impose several requirements on the circuitry driving them. The driver has to supply the forward voltage required even by short wavelength LEDs and LDs and relatively high currents ($\leqslant$ 100 mA) for multiple independent diodes. Additionally stimulation timing and intensity has to be controlled with precision even at high frequencies by analog or digital input signals. Most commercially available drivers are insufficient in at least one of those requirements, and are available only in single or low channel counts.

1.2.3 *Wave guidance*

Targeted light delivery to deep brain structures is routinely achieved by implantation of optical fibers [2, 58]. The efficiency of stimulation however is limited by the conductance and kinetics of the expressed opsins in combination with the capacity of the fiber to deliver suprathreshold intensities within the tissue volume of interest [67]. The opsin activation is determined by the light intensity. The achievable intensity in turn is determined by the efficiency of the light source-fiber coupling and increasing the fiber diameter does not increase the intensity for homogenous waveguides. Highly coherent sources like lasers can be coupled into small diameter single mode fibers [55]. Other light sources require larger diameter fibers [2] to achieve usable light intensities. While the capacity can be increased with higher fiber diameters, a large waveguide size can cause local ischemia and neuronal damage at the implantation site [36].

1.3 CONCURRENT ELECTROPHYSIOLOGY AND OPTOGENETICS

While a large variety of solutions for *in-vivo* electrophysiology in awake behaving animals are available [11], with high channel counts, sampling rate and signal fidelity for both high resolution local field potential (LFP) and unit recordings, optogenetic requirements add new challenges. Several systems for stimulation of deep brain structures and concurrent recording have been described or are commercially available, but most are intended for large scale activation using large diameter fibers, far from the recording electrodes while delivering large amounts of light [58, 55].

Understanding the circuit-level functional organization, development and pathology requires concurrent stimulation of a small set of neurons or circuits and the concurrent recording of electrical activity of affected neurons. Furthermore, some require perturbation of multiple distinct sites in parallel. Recent solutions for such localized light delivery and concurrent recording are limited in the number of independent light paths as they rely on external sources for illumination, constraining the experiment by both rigid and fragile fibers. As many behavioral tasks for freely moving animals emphasize monotonic movement patterns (i.e. circular mazes), this quickly leads to twisting, which greatly increases encumbrance of the animal and can lead to destruction of the fiber [68]. Commutators for both optical and electric connections can offset this for single fibers and low channel counts, but are currently not feasible for more than two fibers.

Here, I describe work published as Stark *et al.* [59] in which the authors placed miniature solid-state light sources on the animals head by coupling them to optical fibers terminating close to the recording electrodes [1, 55]. This approach greatly reduces additional tether as

only a thin flexible electric connection is required. Additionally, this approach can be scaled (albeit the number of fibers and light sources is still limited) and allows highly localized stimulation with great temporal precision and fine tuning of the stimulus intensity.

2

METHODS

2.1 LIGHT DELIVERY

To allow multi-site optogenetic control of concurrently recorded neurons in small laboratory rodents, we manufactured light-weight head-mounted optics by coupling small-diameter waveguides to solid state diode-based light sources (LEDs or LDs). These couplets were glued to tetrodes or the shanks of high-density multi-electrode arrays (MEAs) and mounted on moveable micro-drives. Diode-probe assemblies were implanted into the brains of mice or rats expressing microbial opsins under neuron-specific promoters. To control light intensity with high precision, we built a multi-channel programmable current source that allows to independently stimulate multiple light sources in arbitrary temporal patterns.

2.1.1 *Diode-fiber couplets*

2.1.1.1 *Fiber preparation*

To minimize tissue damage while placing the fiber tip close to the recording sites, step-index multi-mode fibers with small core diameters (50 µm, AFS50/125Y; 105 µm, AFS105/125Y; numerical aperture (NA) 0.22 ± 0.02; Thorlabs) were used. Fibers were cut to length (2–4 cm) with a diamond wedge scribe (S90W; Thorlabs) and 10–12 mm of the acrylate jacket were mechanically removed on one end using a fiber stripping tool (T08S13; Thorlabs).

The cladding diameter of the exposed end was then reduced in discrete steps and the core formed to a pointed tip to further minimize local tissue damage by etching with hydrofluoric acid (HF). The etchant was filled into a small plastic well and covered with a thin layer ($\approx$ 1 mm) of mineral oil. Several fibers were held with a micromanipulator, lowered into the acid and retracted at predetermined times (10 min at 8 mm, 5 min at 5.5 mm, and 15–20 min at 0.5 mm). The resulting stepped profile retained 10–20 µm of cladding at the thinnest section and the tip was over-etched into a cone ($\approx$ 12° half-angle) at the acid/oil interface. The proximal end of the fibers were hand polished with 5 µm lapping sheets (LFG5P; Thorlabs) to a sym-

Note: HF is a very strong corrosive and a contact poison. Handling and use require appropriate care!

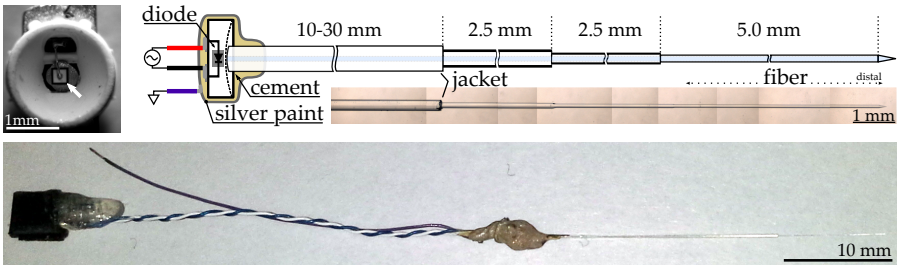

Figure 2: Composition of diode-fiber couplets. The principle of LEDs applies to LDs. *Top left:* Top view of a 2 mm LED (LB P4SG; Osram) with a 250 µm die (white arrow). Note the bonding wire pad in the center. *Top right:* Schema of an LED coupled to a tapered and pointed fiber. *Inset*: Photomosaic of a magnified 125 µm/50 µm core diameter multi-mode fiber showing the removed acrylate jacket (left) and step profile towards the tip at the distal end (right). *Bottom:* Photo of a finished couplet with three light-weight wires for power (white and blue) and grounding of the shielding (violet).

metrical shape. Optionally, the fiber terminal can be polished further following standard fiber preparation procedures.

2.1.1.2 *Diode preparation*

Note: Osram LB P4SG LEDs are distributed with a large spread in individual rated brightness (220–1800 mcd).

LEDs (2 mm round surface mount technology (SMT) package; 470 nm; LB P4SG; OSRAM, 250 µm die side length, Figure 2, bottom) and single- (5.6 mm TO-can package; 639 nm; HL 6359MG; Opnext; or 405 nm) or tri-color (405 nm, 650 nm and 780 nm; SLD6562TL; Sony) LDs were prepared by shortening the leads and manually soldering flexible lightweight wires (3–4 cm) to the respective anode and cathode pads. Soldering times were kept to a minimum to prevent thermal damage, especially for LEDs. To reduce weight and size of laser diodes (5.6 mm laser diode package), the skirt of the metal housing base was cut down to the diameter of the metal can, taking care to minimize mechanical stresses to the laser housing.

The I_f-light power relation of the diodes before, during and after coupling were documented using a calibrated current source (see 2.1.4) and a wavelength-calibrated photodiode power meter (S130A; Thorlabs). These measurements were used to calculate the coupling efficiency (power after coupling divided by initial value) at each step of the assembly process. Diodes with insufficient initial power, output instability or unexpectedly high output losses at any step were discarded.

2.1.1.3 *Alignment and fortification*

During the coupling process, the fiber was kept in a fixed position by a base plate with double-sided adhesive tape mounted on a micromanipulator (figure 3, top, I). The diode was held by a 6-degrees

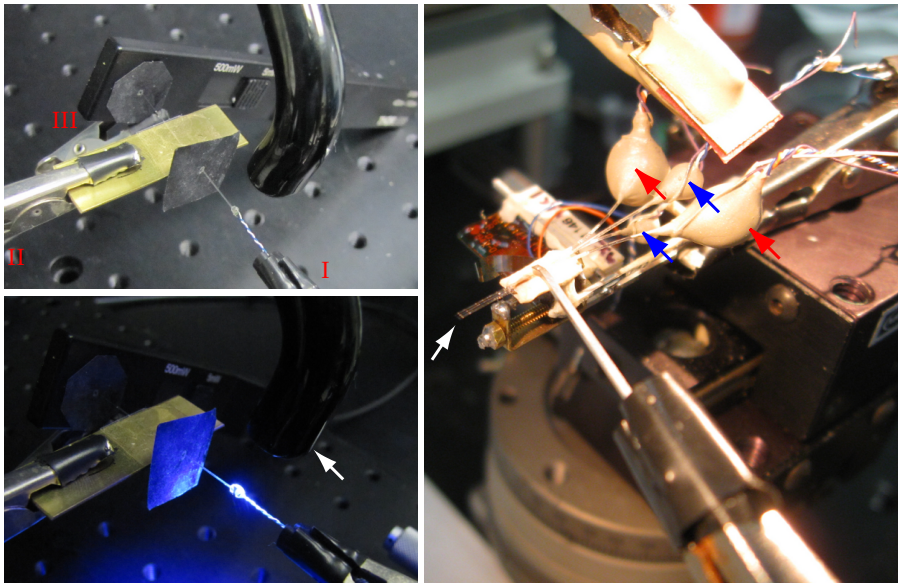

Figure 3: Setups for manufacturing of diode-fiber couplets and mounting those couplets onto silicon probes. Top: Alignment of the prepared LED [I] with the proximal end of an etched optical fiber. The fiber is held by a micro-manipulator and weakly stuck to double sided tape [II]. The photodiode of a light power meter is held close (< 1 mm) to the fiber tip. Bottom: Curing of index-matching glue in the fiber-diode interface with a UV gun (white arrow). Right: Mounting four diodes (two 405.639 nm dual-color laser diodes, red arrows; two 470 nm LEDs, blue arrows) onto a four-shank high-density silicon probe (Buzsaki32P, white arrow) cemented to a moveable micro-drive. A micromanipulator holds the diode and arranges it to be glued onto a shank. The base of the setup can move in a plane and rotate the probe for additional alignment control. A second micromanipulator can optionally be used for fine adjustment of the fiber position.

of freedom (DOF) micro-manipulator perpendicular to the proximal end of the fiber (figure 3, top, II), close enough to generate a visible emission of light from the fiber. The sensor of a photodiode light power meter (PM30 meter; S130A sensor; Thorlabs) was positioned close ($\leqslant 500\,\mu m$) to the distal tip of the fiber using a third micro-manipulator (figure 3, top, III). To prevent illumination by light not originating from the fiber tip, black pieces of paper with pinholes were threaded onto the fiber, shadowing and covering the sensor opening.

After initial setup, the diode position was adjusted in three dimensions to maximize the light power emitted from the fiber tip. Without touching the light source housing, this typically yielded coupling efficiencies of 0.1–0.15 % for LEDs, and $\approx 2.5\,\%$ for laser diodes. A small droplet of UV-curable index-matching adhesive (refractive index (RI) 1.56; NOA-61; Norland Products) was placed between fiber end and diode housing and the diode-position adjusted again. The resulting reduction in Fresnel losses and increase in the acceptance angle for skew rays drastically increased coupling efficiency to $\approx 0.25\,\%$ for LEDs and ≈ 3–$5\,\%$ for laser diodes [59]. The glue was then cured with a UV-gun (ELC-410; Thorlabs) over 10 min from various angles (Figure 3, bottom). A larger drop of glue was added, spread onto the diode housing and cured to increase mechanical stability and prevent the intrusion of cement solvent into the glue/housing interface. The assembly was reinforced with dental cement (Grip cement; Caulk Dentsply). The fortifying layer was added in multiple steps and applied uniformly to avoid deterioration of the alignment by the shrinkage of the cement during solidification. To prevent contact of the following shielding with leads of the diode, electrical insulation quality of the cement layer was checked by immersing the coupled diode-fiber in 0.9 % saline and measuring the impedance at 1 kHz between medium and the shorted leads. Cement was added until $> 15\,M\Omega$ were achieved. A ground wire was attached to the cement with cyanoacrylate glue (454; Loctite). A thin layer of conductive silver paint ($\geqslant 60\,\%$ w.v.; M.E.Taylor Engineering Inc.) was applied as shielding to reduce electromagnetic artifacts and minimize light leakage, thoroughly covering the lead of the ground wire. Insulation quality was checked again and assemblies with markedly reduced impedance were discarded.

2.1.2 *Diode-probe assembly*

Diode-fiber assemblies were glued to silicon probe (e.g., Buzsaki64SP; NeuroNexus) shanks. The procedure of gluing small diameter fibers to silicon probes has been described by [55] and has been modified for diode couplets. First, the probe was cemented onto a micro drive. Micro dives were constructed from rectangular brass frames and a

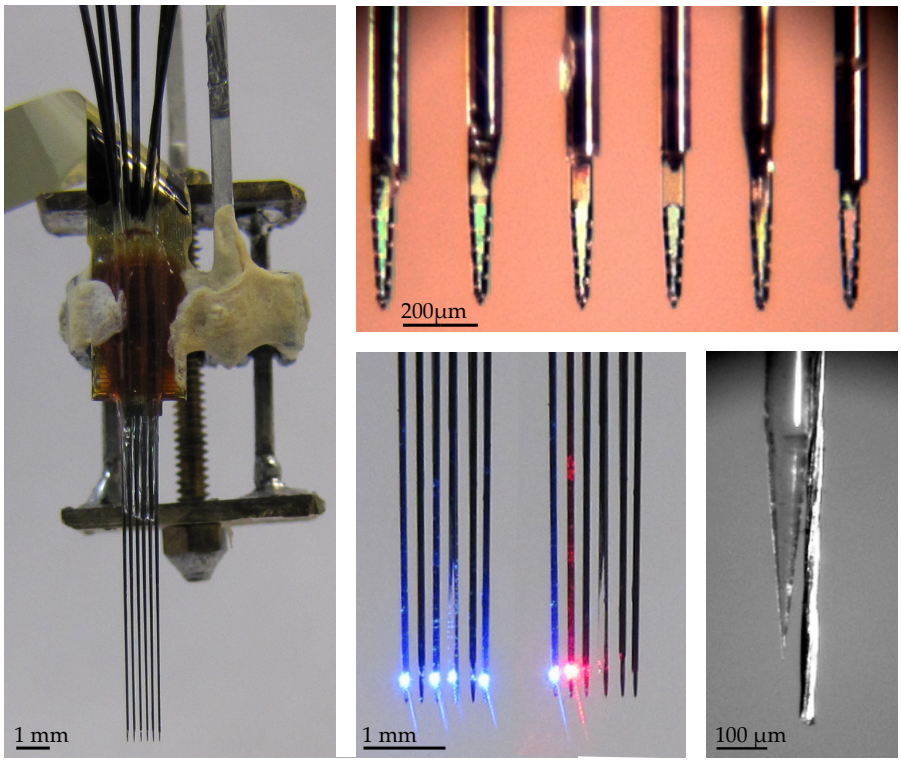

Figure 4: Diode-probes.

tightly fitting threaded plastic sled. Silicon probes and a T-shaped metal bar were cemented to the moveable sled (Figure 4, left). Using two micro-manipulators, fibers and silicon probe shanks were aligned under microscopic guidance to be collinear. The fiber was lowered onto the shank at about 20–30° angle, bending shank until fiber and probe were aligned over the majority of the shank length. The fiber tip was positioned 50 µm above the first recording site (Figure 4, top). Using tetrode wire or single bristles of cotton tips single droplets of UV-curable glue (NOA-61; Norland Products) were placed onto the fiber-probe contact. Care had to be taken to keep the glue from running into the divergence of fiber and silicon at the fiber tip and touch the core, as light would be lost at this point, and to keep glue from covering recording sites. Once alignment initial alignment was satisfactory, the glue was cured for 5–10 min with a UV gun (ELC-410; Thorlabs). The fiber was then slowly retracted to pull the shank into its original plane and the position fixed by gluing both the remaining fiber-probe interspace and the fiber to the probe base. Couplets were mounted sequentially from the lateral to the medial shanks. The diode body was carefully displaced to leave space for following couplets and cemented to the T-shaped bar. Finally, the ground wires were soldered together and power-connections were soldered to small connectors (Millmax) and all fibers and couplets solidly cemented to the drive. Depending on number of couplets and diode type, finished devices weighed 0.5–1 g.

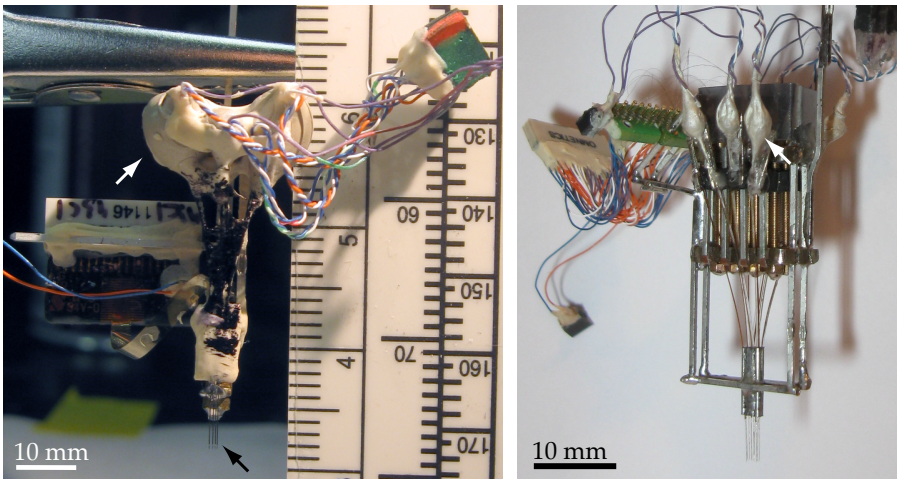

Figure 5: Fully assembled implantation-ready optoelectric arrays. *Left:* 4-shank silicon probe with two 470 nm LEDs and two dual-color LDs (405 nm and 639 nm, arrow) couplets. *Right:* Multi-tetrode drive with 8 wire-tetrodes and up to 8 (here: 6) 470 nm LEDs couplets (arrow).

2.1.3 *Diode-tetrode assembly*

Alternatively, diode-couplets were glued to tetrodes. Tetrodes were manufactured by twisting four 12 µm tungsten wires (California Fine Wire) and melting the insulation with a heat-gun, microscopically checked for faults and then placed into silica tubes (inner/outer diameter 76/153 µm resp.; Polymicro). The tetrode was then aligned with the fiber of a diode coupled. The the fiber tip was positioned $\approx$ 100 µm above the tetrode end (Figure 4, bottom-right). To secure the alignment both were glued in together using UV curable glue (see 2.1.2). The proximal part of the fiber was equally glued to the silica tube, resulting in a combined diameter of $\approx$ 403 µm. Multiple such assemblies were combined on a multi-tetrode drive (Figure 5, left) built as a modified of the silicon probe drive. Each tetrode-assembly was attached to an independent movable sled on a screw and supported by 5–10 mm rods slightly angled to maintain a minimum distance between the diode-couplets. Fiber and tubing were threaded into an array consisting of of 23 american wire-gauge (AWG) stainless steel hypodermic needle tubes in required arrangement. This freely accommodated the assemblies while maintaining precise anatomic positioning. Finally ground and power wires were prepared as in the previous section.

2.1.4 *Programmable multi-channel precision current source*

Each diode was controlled by a separate channel of a custom-built 16-channel programmable linear current source (Figure 6). The choice of a source device over a current sink alternative allows independent

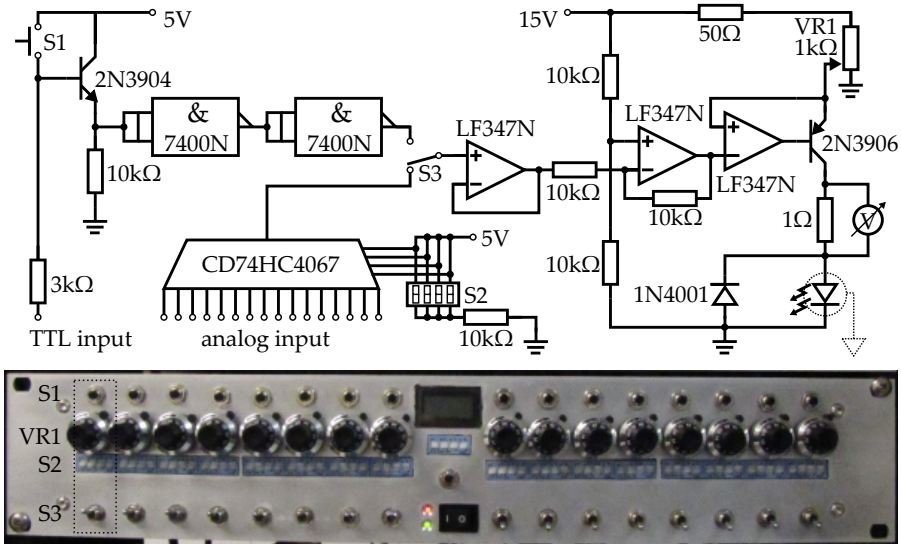

Figure 6: The high-precision multi-channel current source. *Top:* Schematic for a single channel with input stage (left side) and current control stage (right side) driving a single diode (right bottom corner). *Bottom:* View of the front panel. Control elements of a single channel are labeled.

and parallel driving of up to 16 grounded loads with currents of up to 100 mA per channel, while simplifying wiring and allowing programming relative to ground. The circuit was powered by ±18 V regulated bench power supplies. This allowed linear compliance with 0–5 V programming signal and driving of diodes with high forward voltages, such as blue LEDs and LDs. The device consisted of four modules of printed circuit boards (PCBs) carrying circuitry for four channels each, and a 16-channel all-to-all multiplexing board. The multiplexing board allows to arbitrarily select the analog input channel, including selecting the same input channel for multiple diodes, for any of the 16 individual circuits. Source selection is executed by 16-channel analog multiplexer integrated components (ICs) (CD74HC4067) whose input is controlled by 4 bit dual inline package (DIP) switches.

The digital input stage of the circuit consisted of a NPN transistor (2N3904) in emitter-follower configuration, receiving either transistor-transistor logic (TTL) input or manually 5 V from a push button (S1). The signal was then digitally buffered by a non-inverting buffer of two in-series NAND gates with shorted inputs.

Digital or analog input signals were selected by a toggle switch (S2) and buffered by an operational amplifier (op-amp) in voltage-follower configuration. The current control stage consists of an op-amp (LF347N) in differential configuration and a PNP transistor (2N3906) with an op-amp with negative-feedback, using a high-resolution 1 kΩ potentiometer to adjust the maximum allowed current per channel.

For digital control, the current limited was fixed and adjusted for each individual diode (typically 20–60 mA) and the maximum set current switched by the digital output of the digital signal proces-

sor (DSP) (RP2.1; Tucker-Davis Technologies). Analog signals were supplied by the analog output of the DSP or a separate computer-based digital-analog conversion (DAC) card (PCI-6129; National Instruments). A 12-channel lightweight wire (30 AWG; New England Wire Technologies) were used to connect current channels and return paths to diodes on the animal.

2.2 ANIMAL PROCEDURES

All protocols were approved either by the Institutional Animal Care and Use Committee of Rutgers University or New York University.

Animals were housed individually in plastic cages in a temperature ($22 \pm 1\,^{\circ}\mathrm{C}$) and humidity (40–60 %) controlled facility on a 12 h/12 h light/dark schedule. Food and water were available *ad libitum* unless water was restricted for experiments. When on water restriction, body weight was monitored daily and animals provided with water to maintain 90 % *ad libitum* body weight. Additionally, duration of water restriction was limited to 5 days followed by a recovery day with freely accessible water.

2.2.1 *Behavior*

Animals were trained to run for water reward on a fully automated elevated linear track (rats: 150×8 cm, mice: 140×4 cm). The behavioral apparatus was controlled by a programmable DSP (RP2.1; Tucker-Davis Technologies) configured with MATLAB (The MathWorks) via ActiveX. Two solenoid valves (Parker) at either end of the track dispensed de-ionized millipore water (rats: $\approx 50\,\mu$l, mice: $\approx$ 10–20 µl) when the animal passed infrared photoelectric switches (Omron) near the reward platforms after having triggered the previous sensor, requiring it to alternate over the full track length. A third moveable infrared center sensor provided a trigger signal for location dependent light stimulation at a variable position.

2.2.2 *Opsin expression*

2.2.2.1 *Rats*

For experiments using rats, opsin expression was facilitated using recombinant adeno-associated viruses (AAV) locally injected into the target brain region. Vectors were provided by Dr. Karel Svoboda (rAAV2/5 CAG-ChR2-tdTomato; Janelia Farm Research Campus, Howard Hughes Medical Institute) and the University of North Carolina viral core facility (rAAV5 CAG-ChR2-GFP; courtesy of Dr. Ed Boyden; rAAV5 CaMKII-eNPHR3.0-EYFP, courtesy of Dr. Karl Deisseroth [23]), with estimated titers of 10^{12} IU ml^{-1}.

Wild-type Long-Evans rats (300–500 g) were injected with 55 nl viral solution using a microinjector (Nanoject II, Drummond). Animals were placed under isoflourane anaesthesia and the skin over the skull was parted along a small midsigittal cut. Targeting the hippocampal formation, three 200 µm craniotomies were drilled using a dental drill (3.3 ± 0.5 mm posterior-anterior and 3.0 ± 0.5 mm mediolateral). Vector solution was injected in 200 µm intervals along the dorsoventral axis of the hippocampus (CA1: 2.2 ± 0.2 mm dorsoventral; DG: 3.3 ± 0.2 mm; CA3: 3.3 ± 0.2 mm) and the somatosensory cortex (dorsoventral 1.5 ± 0.2 mm). After the injections the scalp was sutured and animals were allowed at least two weeks to recover.

2.2.2.2 *Mice*

For experiments using freely moving mice, two adult male mice were injected with recombinant adeno-associated viruses carrying ChR2 under control of the Calcium/calmodulin-dependent protein kinase type II alpha chain (CaMKIIα) promoter (CaMKIIa-hChR2(h134R)-EYFP). Small amounts of viral solutions (55 nL) were injected into a single small craniotomy −1.6 mm posterior-anterior and 1.1 mm mediolateral relative to bregma at five depths (cortex: 0.7 ± 0.2 mm; CA1: 1.1 ± 0.2 mm dorsoventral; see 2.2.2.1 for procedure). Alternatively, male mice heterozygous for a loxP-ChR2 conditional allele (Rosa-CAG-LSL-ChR2(H134R)-EYFP-WPRE; Ai-32; Allen Institute) were crossbred with homozygous females expressing Cre recombinase [45] under the control of the CaMKIIα or PV promoter (B6.Cg-Tg(Camk2a-cre)T29-1Stl/J and B6;129P2-Pvalb tm1(cre)Arbr/J; The Jackson Laboratory). At eight weeks age transgenic pubs were genotyped and adult transgene positive or virus injected animals chronically implanted with optoelectric arrays.

2.2.3 *Surgery and diode-probe implantation*

Surgery followed common procedures for implantation of multi-channel electrodes in rodents[1]. Animals were put under general isoflurane anesthesia and head fixed in a stereotactic frame (Kopf Inc.) after the skin was shaved and cleaned for surgery. A local analgesic (bupivacaine hydrochloride-epinephrine; Marcaine) was administered subcutaneously before opening a midsaggital cut. The skull was exposed and thoroughly cleaned. Multiple stainless steel screws were inserted (#000-120×1/16; Small Parts; see fig. 7) as anchors into the frontal and parietal bones. For mice, the skull was reinforced with dental acrylic cement, for rats the muscles along the lateral crests were cut and additional screws inserted horizontally. Two screws were inserted above the cerebellum and served as ground and indifferent. A cran-

1 See [62] for a detailed guide.

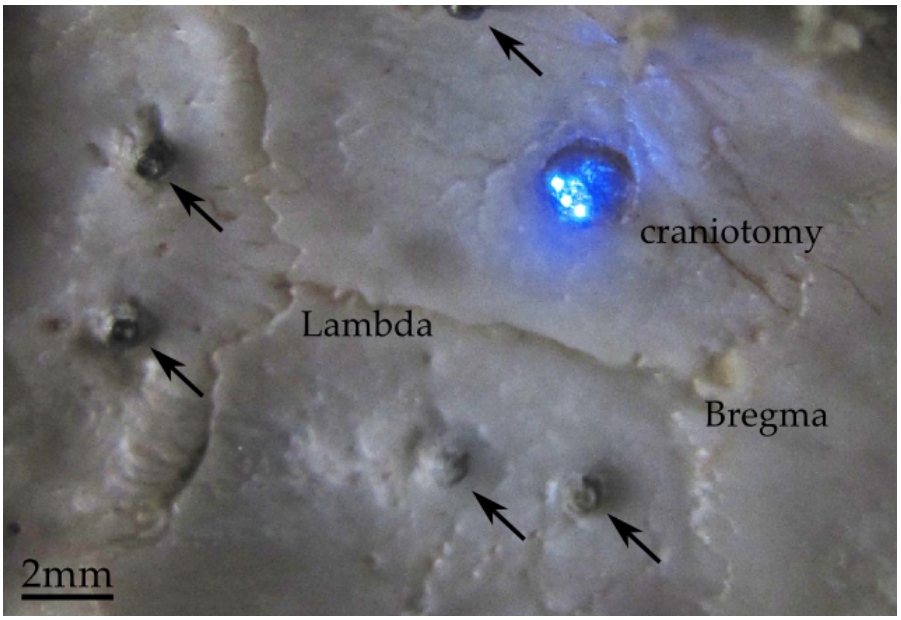

Figure 7: Ventral view of the skull of a rat implanted with a six shank diode-probe after 2 months of recording in the dorsal hippocampus. Three fibers are lit by 470 nm LEDs. Steel anchor screws embedded in the bone are clearly visible (arrows).

iotomy was made and after carefully cleaning the skull periphery the dura mater was nicked and removed. The microdrive carrying the diode-probe assembly was positioned above the opening with stereotactic arm, lowered to about 1 mm above the target structure, and fixed to the skull with dental acrylic (C&B-METABOND; Parkell). The probe shanks and craniotomy were sealed with low-viscosity silicone gel (3-4680; Dow Corning). A grounded copper mesh (3 CU6-050 FA; Dexmet) Faraday cage was built up to the height of drive and headstages and cemented to the skull and anchor screws and reinforced with dental cement (Grip cement; Caulk Dentsply) for mechanical stability. The wound was sutured, and the animal treated with postoperative antibiotics (7.5 mg kg^{-1} enrofloxacin; Baytril) and analgesics (0.05 mg kg^{-1} buprenorphine; Buprenex). During the following 7 days animal were allowed to recover while the probe was slowly moved towards the target position.

2.2.4 *Electrophysiology*

During recording neural activity was examined for spiking, LFP pattern and optical responses online by the experimenter. Neural signals was filtered (1–5000 Hz) and amplified 20× by 32-channel headstages (HST/32V-G20; Plexon) on the animals head, followed by 50× amplification and digitization (16 bit resolution, 20 kHz sampling rate) on a 128-channel direct current (DC) amplifier recording system (Data-

Max; RC Electronics). The system concurrently recorded signals of infrared sensor beam crossings, 3-axis head acceleration, online feature detection triggers and video synchronization signals (see following). Additionally all currents applied to the diodes were recorded via 1 Ω current sensing resistors (Figure 6).

Signals from up to four channels were further band-pass filtered (300–6000 Hz) and amplified (20×), and spikes detected online using amplitude-based windowing (0.15 ms delay, NeuroLog; Digitimer) or detected and sorted using template matching hardware (2.6 ms delay, ASD; Alpha Omega). For online LFP pattern matching, signals were processed using a programmable DSP (RP2.1; Tucker-Davis Technologies) to detect θ (5–11 Hz) activity, power and phase in real time. Triggered digital signals could be used in conjunction with behavioral signals (infrared sensor crossings) to trigger closed-loop stimulation.

The video feed of a CCD camera (Sony) was recorded (Premiere Pro CS1; Adobe). Two LEDs (blue and red, ≈ 8 cm spaced) attached to and powered by the headstages were used to calculate animal position, velocity and heading. The video frames were synchronized to the physiological data from the DataMax system by a current-mirrored LED (green) flashing in regular intervals (≈ 1 Hz) within the field of view of the camera.

2.2.5 *Histology*

Recording site locations were marked by electrolytic lesions. Anodal currents (5 µA, 5–10 s) were injected between two to three sites per probe shank and a rectal steel probe. 24 h later animals were perfused through the left ventricle with 0.9 % saline, followed by 4 % paraformaldehyde in 0.1 M phosphate buffered saline (PBS). Brains were carefully extracted, postfixed overnight and stored in 0.1 M PBS. 80 µm sections were cut with a microtome (Leica). Alternating sections were either Nissl stained for light microscopy, or covered with a protective medium (Vectashield H1400; Vector Laboratories) and coverslipped for fluorescence microscopy (BH2; Olympus).

2.2.6 *Light stimulation*

The established setup allowed to apply arbitrary stimulation patterns by letting DSPs drive the analog input of the current source. Stimuli were constructed as matrices (Matlab, The MathWorks), their correctness checked and uploaded to the DSPs using ActiveX. Once triggered by software or external triggers (sensor crossings, LFP or spike detection feedback) the DSP DACs translated the digital values into voltages controlling the current flow. Conversion sampling rate was typically ≈ 6 kHz or ≈ 50 kHz for closed-loop experiments. Applied currents were monitored and recorded concurrently with the electrophysiol-

ogy signals. For offline power conversion LEDs and LDs were assumed to follow near linear light power/I_f relation. For that purpose LDs were offset by an individually determined I_f threshold.

To assess the effect of light stimulation on spiking of concurrently recorded units we applied rectangular pulses with varying intensity. Pulse intensities were titrated for each site and session by the experimenter to a value that elicited robust spiking without causing spike superpositions. Additionally values above and below the chosen threshold were noted and used for following stimuli to further map response parameter space. Typical stimulation sessions included multiple short duration pulses (1–10 ms) at various frequencies and white noise. For LFP effects and sustained spiking were assessed by rectangular pulses of medium (15–70 ms) and extended durations (up to 400 ms with low duty cycle (D), sine waves of static or dynamically changing frequency, and combinations thereof.

2.2.7 *Data analysis*

2.2.7.1 *Spike detection and sorting*

Spike were detected in the wide-band (1–5000 Hz) signal and their waveforms projected onto a common basis obtained by principle component analysis (PCA) of the data and sorted into single units automatically [28], followed by manual adjustment of the clusters to remove artifacts and reduce over-clustering. Units were required to fulfill the following criteria:

1. amplitude: A minimum peak-to-peak amplitude of 50 µV
2. morphological isolation: $L_{ratio} < 0.05$ [56]
3. temporal isolation: inter-spike interval histogram with clear refractory period (count in the first 2 ms below 0.2 of the expected count given the counts in the first 20 ms [18]

To be included in statistical analysis, units were required to fire at least 100 spikes at a baseline rate over 0.01 spikes s^{-1}. Units were classified as putative pyramidal cells (PYRs) or putative interneurons (INTs) based on short-latency features in baseline cross-correlation histograms [21], responses to DC light pulses (20–70 ms) and/or waveform features.

2.2.7.2 *Effect of light stimulation on spiking*

The time interval during light delivery was defined as the stimulus period. Baseline was defined as the interval three to one stimulus periods before stimulation onset. The spike trains were reduced to 1 ms bins and raster and peri-stimulus time histograms (PSTHs) constructed around the light onset. To further characterize the difference between

stimulated and spontaneous unit activity, the following parameters were calculated:

MEAN FIRING RATE The mean number of spikes per bin during the stimulus period or baseline period, divided by the number of stimuli and bin size.

OPTIMAL INTENSITY The light stimulus strength activating a maximum of targeted cells on the stimulated shank.

GAIN Firing rate during stimulation divided by the baseline firing rate.

LIGHT-MODULATED UNITS Neurons with a significant difference ($P<0.05$; Mann-Whitney U test) in the median number of spikes per bin between stimulus and baseline period over all stimulation trials.

SPIKING PROBABILITY The number of trials with at least one spike during the stimulus period, divided by the total number of trials, calculated for trials with stimulation and for randomized stimulation onset times.

WAVEFORM CONSISTENCY Spike waveforms were recorded on 4–10 sites. Waveforms for each unit and spike were projected onto a common basis obtained by PCA of three eigenvectors per site. Resulting coefficients were averaged as mean waveform description vectors for spikes during stimulation and during baseline. The consistency of the waveform was calculated as the correlation between the description vectors. This consistency measure could then be compared with the recalculated coefficient for randomly permuted spike labels (stimulation and baseline).

LATENCY Time between onset of the stimulus and the first statistically significant bin of the PSTH. Significance was computed by Poisson distribution with Bonferroni correction for the number of bins over the stimulation period.

CENTER-OF-MASS The center-of-mass of spike times (relative to stimulus onset) in significantly high PSTH bins was computed for each trial and averaged over all stimulation trials during which at least one spike was detected over the stimulus period. Significance was determined the same way as for latency.

PRECISION Precision in respect to the stimulus was computed as the standard deviation across trials of the trial-to-trial center-of-mass (see above).

3

RESULTS

3.1 CONSTRUCTION AND CONTROL OF DIODE-PROBES

The constructed current source allows to drive solid-state light sources at high precision and with high temporal resolution. (over 100 kHz with 50 µs rise time for digital input control). While the output signal is highly linear over the majority of the input signal range, at low intensities improper tuning of the channel offsets introduces non-linearities (see figure 16, top left, the sine wave troughs are cut off). The lack of fault detection or prevention circuitry allowed improper input signals to pose risk to the attached components, foremost laser diodes. The output channels of the DSPs, providing digital-to-analog conversion, are in digital HIGH stages until the controllers have been programmed, e.g. after rebooting or after crashes.

Finished LED-fiber couplets weighted 100–120 mg, which depended on the amount of added cement and silver-paint. While the specific light-emitting diodes used were only rated for a maximum I_f of 20 mA [51], we were able to reliably drive them for extended durations (> 10 s) applying currents up to 60 mA. Despite the lack of intended heat bridges for these SMT components, this resulted in only minimal thermal intensity loss and no failed diodes during experimentation. At maximum currents this typically yielded up to 30–45 µW of light at the tip for 50 µm core, 0.22 NA fibers, corresponding to coupling efficiencies of around 0.25 %. At the time of implantation this resulted in 35 ± 7 µW (mean±standard deviation (SD), n=48) blue light at the tip of the fibers. This allows illuminating a brain volume with supra-threshold intensities for ChR2 activation [2, 9] volume of a truncated cone 180 µm by diameter 150 µm of $\approx 1.2 \times 10^{-3}$ mm^3. For blue laser diodes, the intensity of mounted couplets at the point of implantation was 231 ± 62 µW (n=6).

Red laser diodes driven at similar low currents (20–40 mA) reached substantially higher light intensities (100–400 µW, 3–5 % coupling efficiencies). However, laser diodes are inherently susceptible to mechanic or thermal failure and require close control of the forward current to prevent catastrophic optical damage. Additionally, light intensity decline due to heating was much more pronounced due to insufficient cooling. Despite the higher absolute intensities red light

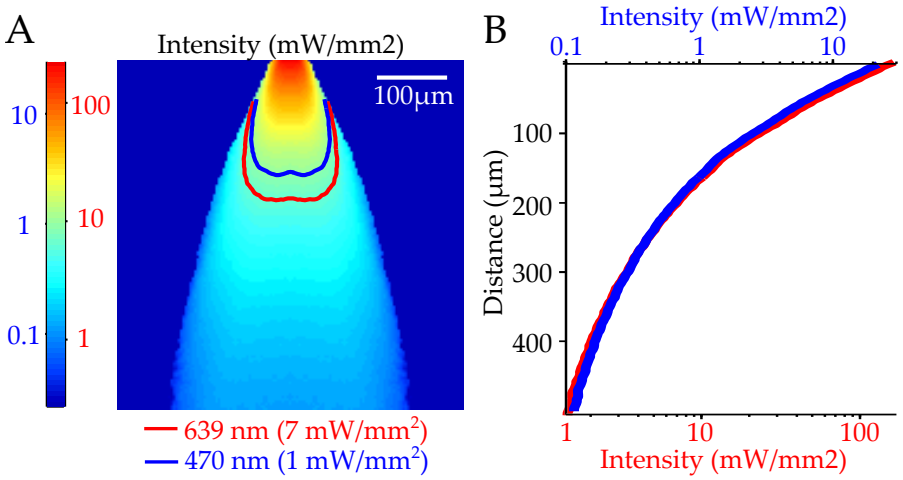

Figure 8: Proposed intensity distribution of 639 nm red light and 470 nm blue light. Proposed ranges for activation of ChR2 (blue lines) and eNpHR3.0 (red lines) activation based on reported activation thresholds. *Left:* Light intensity distribution based on measurements in fluorescin bath [59] for a tipped 50 µm fiber. *Right:* Light intensity as a function of distance from the fiber tip.

stimulation reaches supra-threshold intensities for eNpHR3.0 (Halo) activation ($> 7\,\mathrm{mW\,mm^{-2}}$, [23]) in a similar volume to stimulation with blue LED and ChR2.

The number of illuminated cells is directly proportional to the light intensity of the source, which can be controlled by adjusting the diode current. Assuming cortical and hippocampal cell densities of 20 000–100 000 cells $\mathrm{mm^{-3}}$ [10, 29, 65] this number can be estimated to be in the range of 20–100 cells, many of which can be recorded from MEAs in sufficient quality for isolation and identification [11].

To characterize the effect of localized light stimulation on the spiking activity of cortical and hippocampal neurons, optoelectronic arrays were implanted into mice and rats expressing exogenous opsins under neuron specific promoters. Rats were expressing ChR2 under control of the neuronal cell-type unspecific CAG promoter or Halo specifically in putative excitatory pyramidal cells via the CaMKIIα promoter. Mice were expressing ChR2 under CaMKIIα promoter control in putative interneurons via the PV promoter.

3.2 HISTOLOGY

The efficiency and specificity of expression of the optogenetic constructs was assessed by immuno-labeling and fluorescence of the reporter genes. Unfortunately the CaMKIIα antibody used to label putative pyramidal cells was not working at the time these brains were processed. However, labeling of putative interneurons with PV antibodies shows clear co-localization with EYFP, the ChR2 reporter

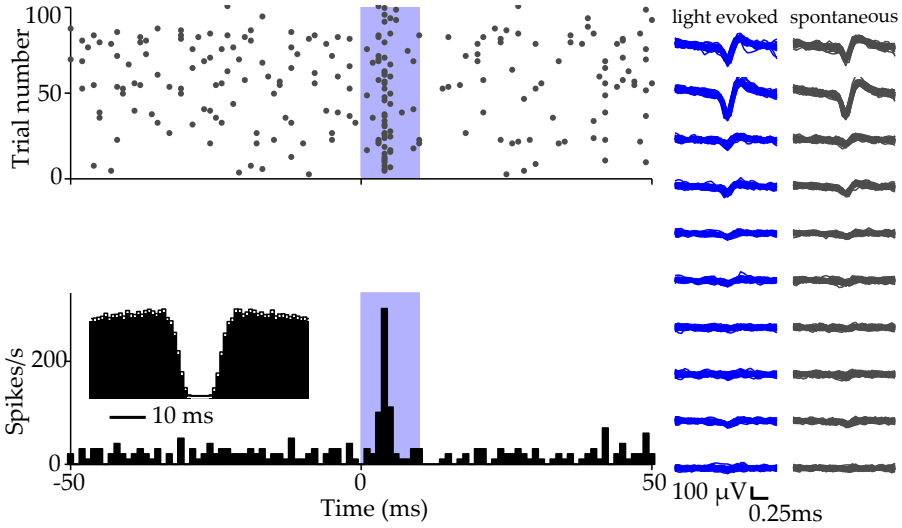

Figure 9: Example of activity modulation of a rat CA1 unit responding to weak light stimulation. 100 stimuli, (rectangular pulse, 10 ms, light power at fiber tip of 4 µW corresponding to intensity of 0.12 mW mm^{-2}, blue background). *Top*: Stimulus onset centered raster plot of spiking of all trials. *Bottom*: PSTH of spiking over all trials. *Inset:* Auto-correlation histogram with clear refractory period. *Right:* Wide-band signals of 10 sites of shank single unit. Spike waveforms were preserved between spontaneous spikes (right) and light-evoked spikes (left, permutation test, P= 0.12)

gene in PV-cre::Ai32 mice, but not in rats unilaterally injected with rAAV5/CamKIIa-hChR2(H134R)-EYFP viral vectors (Figure 10). In PV-cre::Ai32 animals (n=5), all 84 EYFP positive cells were also parvalbumin positive while 84/93 of PV positive cells were EYFP positive (90 %).

Probe tracks were confirmed by tracing tissue damage caused by probe penetration and electrolytic lesioning. In both Nissl and DAPI stainings tracks paths are clearly visible (Figure 11). The shown Nissl stained section is taken from a rat after 2 months of recording with a 6-shank diode-probe, the same animal as the shown skull explant in figure 7. The probe passes through CA1 and the dorsal DG blade. The final position in CA3 is indicated by the electrolytic lesion. Anatomical stainings (Nissl) show no immediate sign of increased tissue damage or local ischemia beyond the extent expected from chronic implantation of rigid electrodes.

3.3 BEHAVIOR

The weight of the implanted drive, including the additional mass of the optical assembly, was less then 10 %$_{\text{b.w.}}$ for all animals, and did not encumber the animals beyond the typical initial accommodation required after implantation. The electrical tether was insignificant rel-

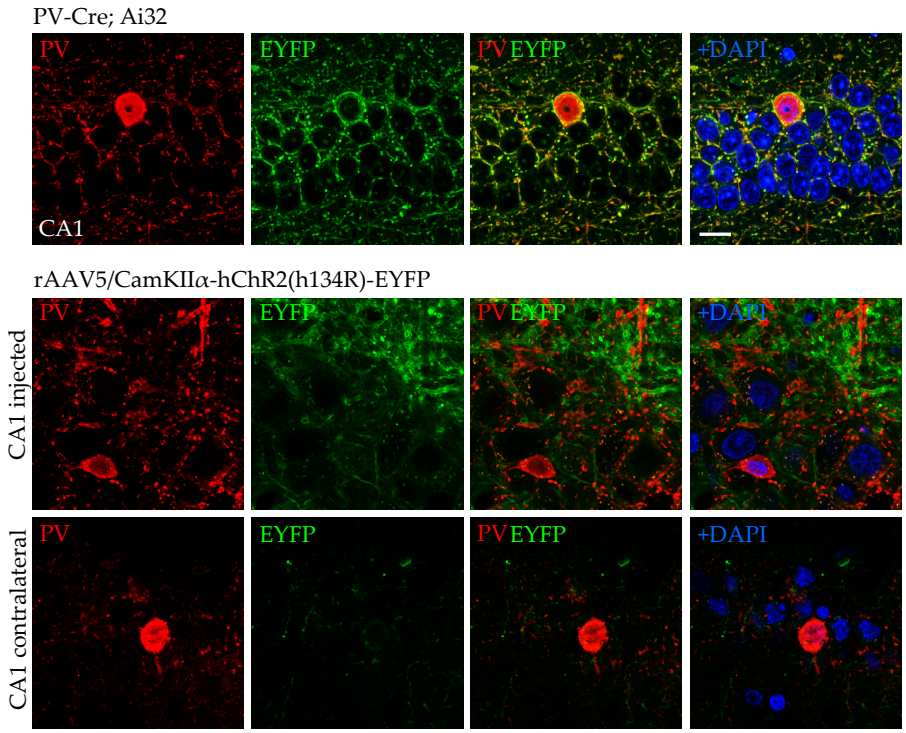

Figure 10: Immunostaining for Parvalbumin (PV) co-localizes with enhanced yellow-fluorescent protein (EYFP), the reporter for channelrhodopsin-2 (ChR2) expression, in PV-Cre::Ai32 mice (*top*), but not in animals unilaterally injected with rAAV5/CamKIIa-hChR2(H134R)-EYFP viruses (*bottom*). DAPI staining shows the presence of pyramidal cells without PV or EYFP labeling. Scale bar: 15 µm

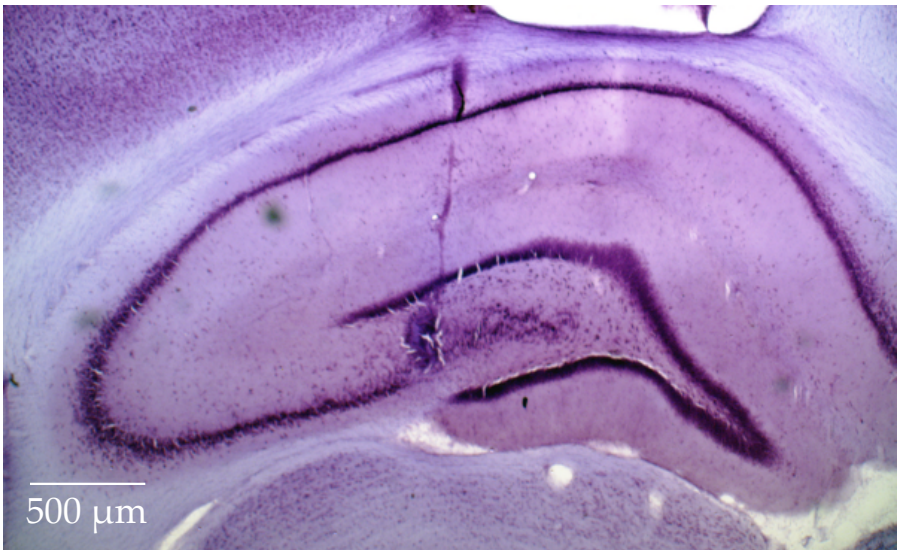

Figure 11: Nissl staining of coronal section of a rat brain after two months recording in dorsal hippocampus. Track passes through CA_1, the dorsal blade of the DG and ends in the CA_3 pyramidal layer with the electrolytic lesion.

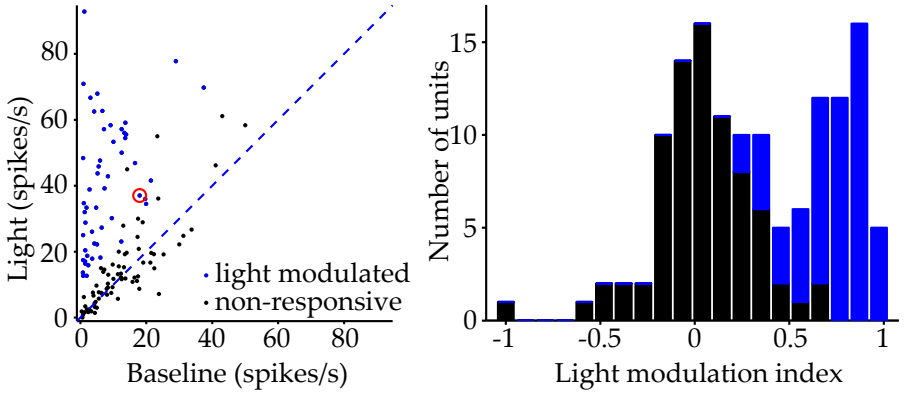

Figure 12: Localized blue light stimulation modulates the firing rate of a substantial population of recorded neurons. *Left:* Spike rates during stimulation versus baseline rates. Red circled unit corresponds to example shown in figure 9. *Right:* Histogram of non-responsive/light modulated units (medians 0.045/0.76; Mann-Whitney U test, $P < 0.001$).

ative to the tether from recording wiring. This preserved behavior, as judged by the experimenter. Animals exhibited a usual palette and frequency of consummatory and exploratory behavior, as well as sleep and grooming during the recording sessions. The degree of freedom preserved is expressed in the good performance during behavioral tasks. Animals ran up to 100 (rats) or 80 (mice) laps in a single session. Mice were easily able to traverse the full length of the narrow linear track (4×140 cm) at high speeds. The average lap duration was 3.5 ± 1.0 s (mean $\pm$ SD).

3.4 STIMULATION EFFICIENCY

The efficiency of stimulating neurons with blue light was characterized in adeno-associated virus (AAV) transduced wild-type rats expressing ChR2 under the CMV early enhancer/chicken beta actin promotor (CAG) promoter. 135 hippocampal and 39 neocortical units met the minimum firing rate requirement and were included in the analysis. Localized low-intensity (3–30 µW at the tip of the fiber, 0.1–1 mW mm^{-2} at the center of the illuminated shank) light stimulation (470 nm, 30 ms median duration rectangular pulses, $D < 0.05$) of neurons in freely moving rats reliably evoked spiking with high spatial and temporal resolution. The firing rate of 42 % of isolated units (57/135 units, 13 shanks recorded in four rats) was stimulation modulated (Mann-Whitney U test, $P < 0.05$) and showed a clear bimodal distribution in modulation indices (Figure 12, right).

The fraction of light-modulated/non-responsive units was not dependent on part of the tested hippocampal structures (CA1, DG, CA3, 0.51/0.38/0.39; χ^2-test, $P = 0.7$).

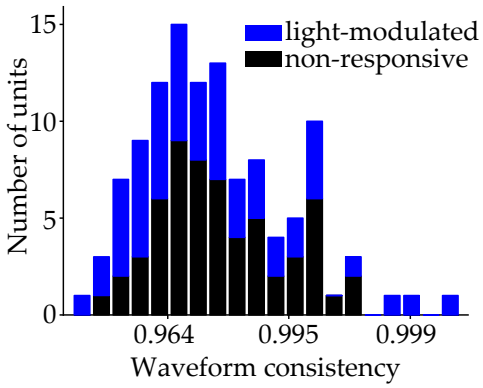

Figure 13: Spike waveforms are preserved for light-modulated and non-responsive units, as measured by correlation between spike description vectors for light/no-light conditions.

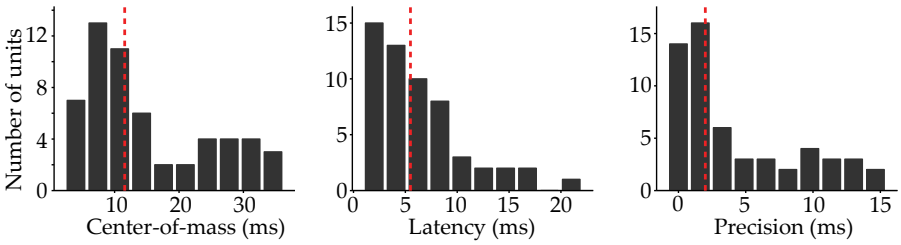

Figure 14: Histograms of timing characteristics of light induced spiking in the CAG::ChR2 expressing wild-type rats during 30 ms (median) rectangular pulses. Dashed red lines represent medians. *Left:* Spiking center-of-mass (CoM) relative to the onset of the stimulus. *Center:* Latency of light induced spiking relative to the stimulus onset. *Right:* Precision of the light-induced spiking response (SD of per-trial CoM).

Despite proximity to the tip of the fiber, all sites were able to record units, even those closest to the fiber (*e.g.* for the unit shown in figure 9 the center-of-mass (CoM) lies across the topmost two proximal sites). This indicates that the substantial additional volume of the fiber does not cause excessive local ischemia or neuronal damage. Light stimulation with weak blue light did not cause superimposition of spikes [55] and spike waveforms were preserved to a high degree (median waveform consistencies for light-modulated/non-responsive units: 0.977/0.986; U test, P= 0.19; figure 13).

3.5 TEMPORAL PRECISION OF INDUCED SPIKING

Spiking response to short rectangular pulses (median 30 ms) in virus-transduced rats (see 3.4) was evoked with a center-of-mass (CoM) (median, 12 ms; n= 57; figure 14 left), latency (median, 5.5 ms; figure 14 center) and precision (median, 2 ms; figure 14 right) within expectations for optogenetic activation of neurons with ChR2 [3, 9]. No difference in spiking latency was observed between the tested regions

in of the hippocampal formation (CA1, DG, CA3; medians 6/6.5/5 ms, Kruskal-Wallis test, P= 0.61)

3.6 SPATIAL RESOLUTION OF ACTIVATION

The spatial extent of neuronal activation was quantified in CA1 (1089 units), where cells are presumed to have few recurrent connections [16, 60] to avoid indirect activation of the investigated cell-type, and neocortex (Cx) (324 units). To further investigate cell-type specific activation, isolated units were classified as putative putative pyramidal cells (PYRs) or putative interneurons (INTs) based on monosynaptic connectivity, light-modulation and/or spike waveform features (for n-numbers see figure 15). Weak light activation with rectangular (DC) pulses (50–70 ms) on single shanks typically elicited spiking limited to the illuminated shank. In CaMKIIα::ChR2 mice (n=4) 33 % (101/309) of locally stimulated pyramidal cells were activated at the optimal level of light (mean 0.56 mW mm^{-2} at the center of the shank). Additionally, a large fraction of interneurons was indirectly activated in a stimulus-intensity dependent manner (Figure 15, left). In contrast, local stimulation in PV::ChR2 mice (n=8) activated a high fraction of locally recorded interneurons (59 % (108/184) at 1.1 mW mm^{-2}), but did not result in activation of non-targeted pyramidal cells (Figure 15, right).

Interestingly, a small fraction of distant pyramidal cells was activated with several fold gain over their baseline firing rate during PV stimulation (Figure 15, right). This might be facilitated by the dis-

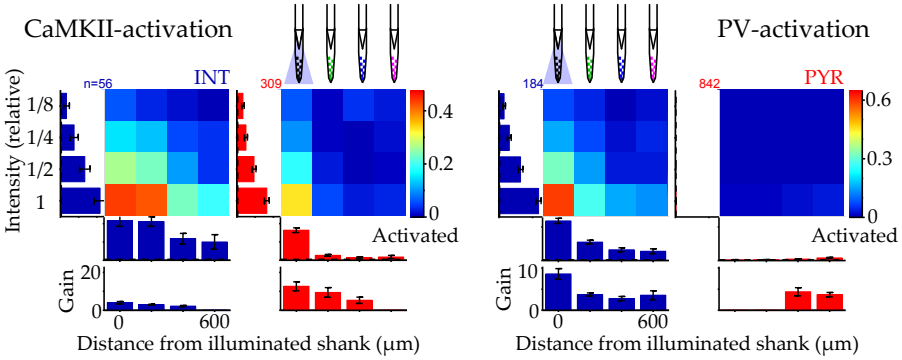

Figure 15: Single-shank stimulation with short (50–70 ms) rectangular pulses results in activation of local cells in CA1 and cortex of mice. Bars represent group means and SEM error bars. Vertical graphs show relative intensity of optimum stimulation strength at the local shank. Horizontal graphs represent fraction of locally activated cells (top) or firing rate gain (bottom). *Left:* Stimulation of CaMKIIα cells activates pyramidal cells locally, and additionally a fraction of interneurons, including distant cells at high intensities. *Right:* Stimulation of PV cells activates interneurons, but not pyramidal cells.

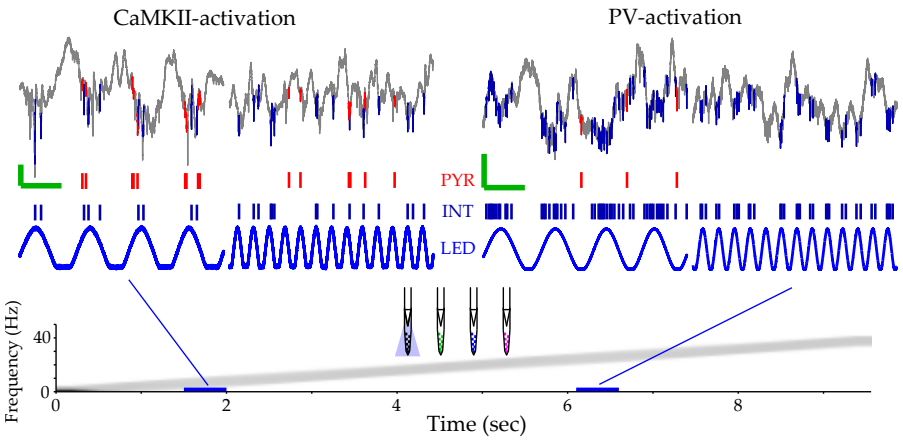

Figure 16: Stimulation with a chirp of linear increasing frequency elicits phase-locked firing. *Top:* Wide-band signal and firing of putative pyramidal cells (PYR, red) and interneurons (INT, blue) in response to the light stimulus, monitored by the current applied to the diode (LED) of two representative segments of the stimulus. *Bottom:* The frequency (0–40 Hz) of the sine wave increases linearly over stimulus period (10 s).

inhibition of pyramidal cells while connected basket cells are inhibited by the locally induced interneuron activity.

Similar results of stimulation locality were obtained by weak light (0.1–0.2 mW mm^{-2}) stimulation in CAG::ChR2 expressing wild-type rats (see 3.4; 3 animals, 10 shanks, 200 µm spacing), where 52 % of locally recorded units responded to light, but distant cells were not activated above baseline (data not shown).

A commonly used signal pattern for investigation of stimulation frequency preferences (e.g. tuning curves) are time-variant sequences like sine-waves, white noise and other complex patterns. Such stimuli can probe the response of a system over a large frequency range within a short period of time, but their application requires high precision control over the stimulation intensity and timing. Here, a sine-wave stimulus with linearly increasing frequency, a "chirp" (Figure 16) is applied. The optogenetic stimulation of neurons elicits spiking with high coherence to the stimulus phase and frequency. During both stimulation of PV and CaMKIIα cells interneurons fired at the peak of the stimulation, but at much higher frequency during direct activation. Pyramidal cells in contrast were activated at the stimulus peak when stimulated directly, but fired close to the trough of the stimulus during PV stimulation (Figure 16, top right).

4

DISCUSSION

Optogenetics is progressing fast, with new advances in opsin technology improving temporal control, activation kinetics, cell specific expression and intracellular trafficking. Current stimulation methodology limitations for *in vivo* local control, using large external light sources and high intensities. To allow activating and concurrent recording of small but defined volumes of neural tissue, close integration of light source and recording electrode is required. To facilitate a scalable approach while maintaining recording quality and stimulation precision, we combined miniature diode based light sources with fiber optical waveguides integrated in the recording electrode arrays. These devices were then implanted into the brains of opsin expressing rodents.

A substantial fraction of recorded and isolated units were modulated by the light stimulation. One reason for this is likely the high transduction rate achieved by recombinant AAV vectors (40–80 % [12]). While the histological characterization of the expression in CaMKIIα animals is incomplete, the robust response achieved in these animals, even at minimal intensities, leaves little doubt about the successful delivery of the opsins. Secondly, the close positioning ($\geqslant 50\,\mu m$) of the fiber tip relative to the recording sites and recorded units are contributing. While fibers have a several-fold cross-section of silicon probes, the close placement of the fiber tips to the neurons did not prevent event the most proximal electrode sites from contributing to the recording. This indicates that the additional neuronal damage does not deteriorate the recording quality. The stimulation of the microbial opsins also seemed to leave the spike shape of the neurons unaffected as spike waveforms were highly conserved. While the quality of the spikes was not affected acutely, the expression of opsins has recently raised alarm to cause long-term changes in the neuronal morphology and connectivity [47]. Further analysis to isolate a possible differences in regards to the expression system and duration is currently underway.

The analysis of the spatial extent unit activation demonstrated the ability to stimulate specific types of cells in a well defined localized volume with a resolution on the scale of the fiber spread ($\approx 200\,\mu m$). The range of activation could be controlled by the stimulus intensity,

and was similar to the expected light distribution. This allows allows to dissect the differential contributions of distributed cells to neuronal circuits and circuit phenomena.

While stimulation with blue LEDs generally achieved good results, the principally superior light power of laser diodes not provide the expected advantage. The available wavelengths at the required power levels only barely match common optogenetic probes. Blue laser diodes typically emit light at 405 nm, which is deep violet and far from the peak activation frequency for ChR2. This requires approximately a ten-fold intensity over 470 nm light to compensate for the spectral offset and the reduced tissue penetration. While the higher output of laser diodes and higher coupling efficiency makes them viable options, the majority of the potential of LDs is wasted. Recently diodes with 450 nm have become available, but are difficult to source at the time of writing.

For Halo with a activation peak wavelength in yellow, the situation is more difficult for LEDs based light sources. While even stimulation with 640 nm red laser diodes achieved effects only at high power, currently there are no LEDs that can provide the power density required to drive Halo efficiently, especially when coupled into small diameter fibers to, despite available color-matching diodes. Ideally, yellow laser diodes should be used for this purpose, especially when inhibiting larger populations or structures. However, laser diode technology is limited by the available semiconductor materials with the required energy band-gaps. Currently, this technology does not exist. Other hyperpolarizing optogenetic probes have similar excitation spectra from yellow-green (Arch) to green-blue (Mac/eBR), but can alleviate this problem by achieving higher photo-currents and lower activation thresholds. As with blue laser diodes, the addition to the range of available compact and high powered diodes will likely expand, and the continued evolution of diode-technology will continue to support the close integration of light sources.

Coupling small diode light sources (i.e. laser- or light-emitting diodes) to small core fibers yields sufficient light to perturb the volume recorded by current electrophysiology technology and causes minimal recording artifacts. Both types of diodes (LEDs and LDs) have are fast switching. Both, but especially LEDs have excellent stability. Many DPSS lasers suffer from fluctuating power levels, speckle noise and mode hopping, and may require mechanical shutters and neutral density filters to regulate intensity reliably. For experiments involving long stimulation periods (e.g. tonic inhibition) or stimulation with high duty cycles however, the unmediated heating of head-mounted diodes can be a limiting factor.

As far as the current source design is concerned, the possibility of damaging the attached optical assemblies, albeit very small, has to be addressed in future iterations. To solve the mismatch in default states

of driving hardware and the current source input, the incoming signal of the analog stage could be inverted, and the signal line pulled high. A digital HIGH signal erroneously applied by the DAC would no longer cause a current to be applied. However, this approach is vulnerable to accidental short circuits of the signal and ground. An alternate, yet more complex solution is the inclusion of fault-state detecting circuitry, which could temporarily disable the input stages to prevent damage. Furthermore the demonstrated non-linearity (16) in the DAC-to-current step likely reflects improper tuning of individual channels and is easily correct, or can be dealt with by offsetting generated signals for selected channels.

4.1 OUTLOOK

The demonstrated hardware allows independent optogenetic control at multiple sites. The range of activation can be adjusted through the intensity of the applied stimulus. This provides a high spatial resolution for analyzing neuronal circuits. The combination of high density electrode arrays with head mounted diodes for light delivery allows application in freely moving animals. This scalable approach only adds minimal additional weight and tethering encumbrance. Given that the majority of necessary components are already miniaturized, it lends itself to fully wireless operation. The circuitry involved simplified and reduced in size, and the high-efficiency light sources would have moderate power requirements, allowing to place the necessary stimulation control and power source on freely moving animals, even mice, where implant size has close weight limits.

The largest contributor to weight is not the probe assembly itself, but the larger hat required by the height of the diode-fibers. The height of the copper mesh hat requires to be reinforced, otherwise hats tend to crumble during long recording (>4 weeks). With care, the copper mesh can be reinforced with cement at strategically chosen segments. For the future, alternative materials should be considered. Initial experiments with carbon fiber crowns were promising given the light weight of the composite. Combined with a finer shielding mesh, the mass of the protective hat can be decreased while simultaneously increasing resilience. However, assembly of the composite during surgery requires substantially more experience by the experimenter. Alternatively, the fiber length can be reduced to shorten the overall height of the probe assembly. Given the high power density of the diodes, we experienced electromagnetic artifacts when the fiber length was reduced too much. This might be attributed to insufficient shielding around the diodes by the silver paint layer, and can most likely be improved. The transient artifacts are troublesome for LFP analysis. For experiments primarily investigating spiking, this may be an acceptable trade-off.

The manual assembly limits feasibility to experiments involving small numbers of animals. The recovery of implanted probes is difficult as the devices are extremely fragile, but can be worthwhile. On the other hand, manual assembly offers the flexibility to adapt optics and fiber arrangement to the scientific question. High-density silicon probes with integrated wave guides or even LED based light sources are in development by a number of groups and should be available for initial testing within the next years [33, 37, 46, 54, 64]. The availability to the general science community however will most likely not be achieved within the next decade, especially considering that tetrodes are still preferred over silicon probes (cost effectiveness being a major factor). While integrated light guides and sources offer tremendous potential, the described method of manufactured fiber-diode couplets combined with proven electrophysiology tools can provide an easy to use and highly versatile complementary approach that can empower researchers to investigate circuit dynamics with high precision.

BIBLIOGRAPHY

[1] Polina Anikeeva, Aaron S Andalman, Ilana Witten, Melissa Warden, Inbal Goshen, Logan Grosenick, Lisa a Gunaydin, Loren M Frank, and Karl Deisseroth. Optetrode: a multichannel readout for optogenetic control in freely moving mice. *Nature neuroscience*, 15(1):163–70, January 2012. ISSN 1546-1726. doi: 10.1038/nn.2992. URL http://www.ncbi.nlm.nih.gov/pubmed/22138641. (Cited on pages 1 and 6.)

[2] Alexander M Aravanis, Li-Ping Wang, Feng Zhang, Leslie a Meltzer, Murtaza Z Mogri, M Bret Schneider, and Karl Deisseroth. An optical neural interface: in vivo control of rodent motor cortex with integrated fiberoptic and optogenetic technology. *Journal of neural engineering*, 4(3):S143–56, September 2007. ISSN 1741-2560. doi: 10.1088/1741-2560/4/3/S02. URL http://www.ncbi.nlm.nih.gov/pubmed/17873414. (Cited on pages 4, 6, and 23.)

[3] Benjamin R Arenkiel, Joao Peca, Ian G Davison, Catia Feliciano, Karl Deisseroth, George J Augustine, Michael D Ehlers, and Guoping Feng. In vivo light-induced activation of neural circuitry in transgenic mice expressing channelrhodopsin-2. *Neuron*, 54(2):205–18, April 2007. ISSN 0896-6273. doi: 10.1016/j.neuron.2007.03.005. URL http://www.ncbi.nlm.nih.gov/pubmed/17442243. (Cited on page 28.)

[4] Christian Bamann, Taryn Kirsch, Georg Nagel, and Ernst Bamberg. Spectral characteristics of the photocycle of channelrhodopsin-2 and its implication for channel function. *Journal of molecular biology*, 375(3):686–94, January 2008. ISSN 1089-8638. doi: 10.1016/j.jmb.2007.10.072. URL http://www.ncbi.nlm.nih.gov/pubmed/18037436. (Cited on page 2.)

[5] Christian Bamann, Georg Nagel, and Ernst Bamberg. Microbial rhodopsins in the spotlight. *Current opinion in neurobiology*, 20(5):610–6, October 2010. ISSN 1873-6882. doi: 10.1016/j.conb.2010.07.003. URL http://www.ncbi.nlm.nih.gov/pubmed/20691581. (Cited on page 2.)

[6] E Bamberg, J Tittor, and D Oesterhelt. Light-driven proton or chloride pumping by halorhodopsin. *Proceedings of the National Academy of Sciences of the United States of America*, 90(2):639–43, January 1993. ISSN 0027-8424. URL http://www.pubmedcentral.nih.gov/articlerender.fcgi?

artid=45719&tool=pmcentrez&rendertype=abstract. (Cited on page 3.)

[7] Francesco P Battaglia, Tobias Kalenscher, Henrique Cabral, Jasper Winkel, Jeroen Bos, Ron Manuputy, Theo van Lieshout, Frans Pinkse, Harry Beukers, and Cyriel Pennartz. The Lantern: an ultra-light micro-drive for multi-tetrode recordings in mice and other small animals. *Journal of neuroscience methods*, 178(2):291–300, April 2009. ISSN 1872-678X. doi: 10.1016/j.jneumeth.2008.12.024. URL http://www.ncbi.nlm.nih.gov/pubmed/19152807. (Cited on page 1.)

[8] Jacob G Bernstein and Edward S Boyden. Optogenetic tools for analyzing the neural circuits of behavior. *Trends in cognitive sciences*, 15(12):592–600, December 2011. ISSN 1879-307X. doi: 10.1016/j.tics.2011.10.003. URL http://www.pubmedcentral.nih.gov/articlerender.fcgi?artid=3225502&tool=pmcentrez&rendertype=abstract. (Cited on page 1.)

[9] Edward S Boyden, Feng Zhang, Ernst Bamberg, Georg Nagel, and Karl Deisseroth. Millisecond-timescale, genetically targeted optical control of neural activity. *Nature neuroscience*, 8(9):1263–8, September 2005. ISSN 1097-6256. doi: 10.1038/nn1525. URL http://www.ncbi.nlm.nih.gov/pubmed/16116447. (Cited on pages 1, 2, 3, 23, and 28.)

[10] Valentino Braitenberg and Almut Schüz. Cortical Architectonics. In *Cortex: Statistics and Geometry of Neuronal Connectivity SE - 27*, pages 135–137. Springer Berlin Heidelberg, 1998. ISBN 978-3-662-03735-5. doi: 10.1007/978-3-662-03733-1_27. URL http://dx.doi.org/10.1007/978-3-662-03733-1_27. (Cited on page 24.)

[11] György Buzsáki. Large-scale recording of neuronal ensembles. *Nature neuroscience*, 7(5):446–51, May 2004. ISSN 1097-6256. doi: 10.1038/nn1233. URL http://www.ncbi.nlm.nih.gov/pubmed/15114356. (Cited on pages 6 and 24.)

[12] Jessica a Cardin, Marie Carlén, Konstantinos Meletis, Ulf Knoblich, Feng Zhang, Karl Deisseroth, Li-Huei Tsai, and Christopher I Moore. Targeted optogenetic stimulation and recording of neurons in vivo using cell-type-specific expression of Channelrhodopsin-2. *Nature protocols*, 5(2):247–54, February 2010. ISSN 1750-2799. doi: 10.1038/nprot.2009.228. URL http://www.ncbi.nlm.nih.gov/pubmed/20134425. (Cited on pages 4 and 31.)

[13] Matt Carter and Jennifer Shieh. *Guide to research techniques in neuroscience*. Academic Press, 2009. (Cited on page 1.)

[14] Matthew E Carter and Luis de Lecea. Optogenetic investigation of neural circuits in vivo. *Trends in molecular medicine*, 17(4):197–206, April 2011. ISSN 1471-499X. doi: 10.1016/j.molmed.2010.12.005. URL http://www.pubmedcentral.nih.gov/articlerender.fcgi?artid=3148823&tool=pmcentrez&rendertype=abstract. (Cited on pages 1 and 2.)

[15] Brian Y Chow, Xue Han, Allison S Dobry, Xiaofeng Qian, Amy S Chuong, Mingjie Li, Michael a Henninger, Gabriel M Belfort, Yingxi Lin, Patrick E Monahan, and Edward S Boyden. High-performance genetically targetable optical neural silencing by light-driven proton pumps. *Nature*, 463(7277):98–102, January 2010. ISSN 1476-4687. doi: 10.1038/nature08652. URL http://www.pubmedcentral.nih.gov/articlerender.fcgi?artid=2939492&tool=pmcentrez&rendertype=abstract. (Cited on pages 1 and 3.)

[16] J Deuchars and A.M. Thomson. CA1 pyramid-pyramid connections in rat hippocampus in vitro: Dual intracellular recordings with biocytin filling. *Neuroscience*, 74(4):1009–1018, October 1996. ISSN 03064522. doi: 10.1016/0306-4522(96)00251-5. URL http://www.ncbi.nlm.nih.gov/pubmed/8895869http://linkinghub.elsevier.com/retrieve/pii/0306452296002515. (Cited on page 29.)

[17] David Fan, Dylan Rich, Tahl Holtzman, Patrick Ruther, Jeffrey W Dalley, Alberto Lopez, Mark a Rossi, Joseph W Barter, Daniel Salas-Meza, Stanislav Herwik, Tobias Holzhammer, James Morizio, and Henry H Yin. A wireless multi-channel recording system for freely behaving mice and rats. *PloS one*, 6(7):e22033, January 2011. ISSN 1932-6203. doi: 10.1371/journal.pone.0022033. URL http://www.pubmedcentral.nih.gov/articlerender.fcgi?artid=3134473&tool=pmcentrez&rendertype=abstract. (Cited on page 1.)

[18] Michale S Fee, Partha P Mitra, and David Kleinfeld. Automatic sorting of multiple unit neuronal signals in the presence of anisotropic and non-Gaussian variability. *Journal of neuroscience methods*, 69(2):175–88, November 1996. ISSN 0165-0270. doi: 10.1016/S0165-0270(96)00050-7. URL http://www.ncbi.nlm.nih.gov/pubmed/8946321. (Cited on page 20.)

[19] Lief Fenno, Ofer Yizhar, and Karl Deisseroth. The development and application of optogenetics. *Annual review of neuroscience*, 34:389–412, January 2011. ISSN 1545-4126. doi: 10.1146/annurev-neuro-061010-113817. URL http://www.ncbi.nlm.nih.gov/pubmed/21692661. (Cited on page 1.)

[20] Stephen Fry. *The Liar*. Heinemann, 1991. ISBN 0434271918. (Cited on page ix.)

[21] Shigeyoshi Fujisawa, Asohan Amarasingham, Matthew T Harrison, and György Buzsáki. Behavior-dependent short-term assembly dynamics in the medial prefrontal cortex. *Nature neuroscience*, 11(7):823–33, July 2008. ISSN 1097-6256. doi: 10.1038/nn.2134. URL http://www.pubmedcentral.nih.gov/articlerender.fcgi?artid=2562676&tool=pmcentrez&rendertype=abstract. (Cited on page 20.)

[22] Viviana Gradinaru, Kimberly R Thompson, and Karl Deisseroth. eNpHR: a Natronomonas halorhodopsin enhanced for optogenetic applications. *Brain cell biology*, 36(1-4):129–39, August 2008. ISSN 1559-7113. doi: 10.1007/s11068-008-9027-6. URL http://www.pubmedcentral.nih.gov/articlerender.fcgi?artid=2588488&tool=pmcentrez&rendertype=abstract. (Cited on page 3.)

[23] Viviana Gradinaru, Feng Zhang, Charu Ramakrishnan, Joanna Mattis, Rohit Prakash, Ilka Diester, Inbal Goshen, Kimberly R Thompson, and Karl Deisseroth. Molecular and cellular approaches for diversifying and extending optogenetics. *Cell*, 141 (1):154–65, April 2010. ISSN 1097-4172. doi: 10.1016/j.cell.2010.02.037. URL http://www.ncbi.nlm.nih.gov/pubmed/20303157. (Cited on pages 2, 3, 16, and 24.)

[24] Lisa a Gunaydin, Ofer Yizhar, André Berndt, Vikaas S Sohal, Karl Deisseroth, and Peter Hegemann. Ultrafast optogenetic control. *Nature neuroscience*, 13(3):387–92, March 2010. ISSN 1546-1726. doi: 10.1038/nn.2495. URL http://www.ncbi.nlm.nih.gov/pubmed/20081849. (Cited on pages 1 and 3.)

[25] Roland Haitz. Haitz's law. *Nature Photonics*, 1(1):23–23, January 2007. ISSN 1749-4885. doi: 10.1038/nphoton.2006.78. URL http://dx.doi.org/10.1038/nphoton.2006.78http://www.nature.com/doifinder/10.1038/nphoton.2006.78. (Cited on page 5.)

[26] Xue Han and Edward S Boyden. Multiple-color optical activation, silencing, and desynchronization of neural activity, with single-spike temporal resolution. *PloS one*, 2(3):e299, January 2007. ISSN 1932-6203. doi: 10.1371/journal.pone.0000299. URL http://www.pubmedcentral.nih.gov/articlerender.fcgi?artid=1808431&tool=pmcentrez&rendertype=abstract. (Cited on page 2.)

[27] Xue Han, Brian Y Chow, Huihui Zhou, Nathan C Klapoetke, Amy Chuong, Reza Rajimehr, Aimei Yang, Michael V Baratta,

Jonathan Winkle, Robert Desimone, and Edward S Boyden. A high-light sensitivity optical neural silencer: development and application to optogenetic control of non-human primate cortex. *Frontiers in systems neuroscience*, 5(April):18, January 2011. ISSN 1662-5137. doi: 10.3389/fnsys.2011.00018. URL http://www.pubmedcentral.nih.gov/articlerender.fcgi?artid=3082132&tool=pmcentrez&rendertype=abstract. (Cited on page 3.)

[28] Kenneth D Harris, Darrell A Henze, Jozsef Csicsvari, Hajime Hirase, and G Buzsáki. Accuracy of tetrode spike separation as determined by simultaneous intracellular and extracellular measurements. *Journal of neurophysiology*, 84(1):401–14, July 2000. ISSN 0022-3077. URL http://www.ncbi.nlm.nih.gov/pubmed/10899214. (Cited on page 20.)

[29] Mohammad Hosseini-Sharifabad and Jens Randel Nyengaard. Design-based estimation of neuronal number and individual neuronal volume in the rat hippocampus. *Journal of neuroscience methods*, 162(1-2):206–14, May 2007. ISSN 0165-0270. doi: 10.1016/j.jneumeth.2007.01.009. URL http://www.ncbi.nlm.nih.gov/pubmed/17368561. (Cited on page 24.)

[30] A Idnurm and B J Howlett. Characterization of an opsin gene from the ascomycete Leptosphaeria maculans. *Genome / National Research Council Canada = Génome / Conseil national de recherches Canada*, 44(2):167–71, April 2001. ISSN 0831-2796. URL http://www.ncbi.nlm.nih.gov/pubmed/11341726. (Cited on page 3.)

[31] Justin Iveland, Lucio Martinelli, Jacques Peretti, James S Speck, and Claude Weisbuch. Direct Measurement of Auger Electrons Emitted from a Semiconductor Light-Emitting Diode under Electrical Injection: Identification of the Dominant Mechanism for Efficiency Droop. *Physical Review Letters*, 110(17):177406, April 2013. ISSN 0031-9007. doi: 10.1103/PhysRevLett.110.177406. URL http://arxiv.org/abs/1304.5469http://link.aps.org/doi/10.1103/PhysRevLett.110.177406. (Cited on page 5.)

[32] S KARNIK, C GOGONEA, S PATIL, Y SAAD, and T TAKEZAKO. Activation of G-protein-coupled receptors: a common molecular mechanism. *Trends in Endocrinology and Metabolism*, 14(9):431–437, November 2003. ISSN 10432760. doi: 10.1016/j.tem.2003.09.007. URL http://linkinghub.elsevier.com/retrieve/pii/S1043276003001917. (Cited on page 2.)

[33] Tae-il Kim, Jordan G McCall, Yei Hwan Jung, Xian Huang, Edward R Siuda, Yuhang Li, Jizhou Song, Young Min Song, Hsuan An Pao, Rak-Hwan Kim, Chaofeng Lu, Sung Dan Lee,

Il-Sun Song, Gunchul Shin, Ream Al-Hasani, Stanley Kim, Meng Peun Tan, Yonggang Huang, Fiorenzo G Omenetto, John a Rogers, and Michael R Bruchas. Injectable, cellular-scale optoelectronics with applications for wireless optogenetics. *Science (New York, N.Y.)*, 340(6129):211–6, April 2013. ISSN 1095-9203. doi: 10.1126/science.1232437. URL http://www.ncbi.nlm.nih.gov/pubmed/23580530. (Cited on pages 4 and 34.)

[34] Richard H Kramer, Doris L Fortin, and Dirk Trauner. New photochemical tools for controlling neuronal activity. *Current opinion in neurobiology*, 19(5):544–52, October 2009. ISSN 1873-6882. doi: 10.1016/j.conb.2009.09.004. URL http://www.pubmedcentral.nih.gov/articlerender.fcgi?artid=2788492&tool=pmcentrez&rendertype=abstract. (Cited on page 2.)

[35] Alexxai V Kravitz and Anatol C Kreitzer. Optogenetic manipulation of neural circuitry in vivo. *Current opinion in neurobiology*, 21(3):433–9, June 2011. ISSN 1873-6882. doi: 10.1016/j.conb.2011.02.010. URL http://www.pubmedcentral.nih.gov/articlerender.fcgi?artid=3130851&tool=pmcentrez&rendertype=abstract. (Cited on page 1.)

[36] Alexxai V Kravitz, Benjamin S Freeze, Philip R L Parker, Kenneth Kay, Myo T Thwin, Karl Deisseroth, and Anatol C Kreitzer. Regulation of parkinsonian motor behaviours by optogenetic control of basal ganglia circuitry. *Nature*, 466(7306):622–6, July 2010. ISSN 1476-4687. doi: 10.1038/nature09159. URL http://www.pubmedcentral.nih.gov/articlerender.fcgi?artid=3552484&tool=pmcentrez&rendertype=abstract. (Cited on page 6.)

[37] K. Kwon and W. Li. Integrated multi-LED array with three-dimensional polymer waveguide for optogenetics. In *2013 IEEE 26th International Conference on Micro Electro Mechanical Systems (MEMS)*, pages 1017–1020. IEEE, January 2013. ISBN 978-1-4673-5655-8. doi: 10.1109/MEMSYS.2013.6474421. URL http://ieeexplore.ieee.org/lpdocs/epic03/wrapper.htm?arnumber=6474421. (Cited on page 34.)

[38] J K Lanyi. Halorhodopsin: a light-driven chloride ion pump. *Annual review of biophysics and biophysical chemistry*, 15(17):11–28, January 1986. ISSN 0883-9182. doi: 10.1146/annurev.bb.15.060186.000303. URL http://www.ncbi.nlm.nih.gov/pubmed/7604281. (Cited on page 3.)

[39] Janos K. Lanyi and Brigitte Schobert. Effects of chloride and pH on the chromophore and photochemical cycling of

halorhodopsin. *Biochemistry*, 22(11):2763–2769, May 1983. ISSN 0006-2960. doi: 10.1021/bi00280a026. URL http://pubs.acs.org/doi/abs/10.1021/bi00280a026. (Cited on page 3.)

[40] John Y Lin. A user's guide to channelrhodopsin variants: features, limitations and future developments. *Experimental physiology*, 96(1):19–25, January 2011. ISSN 1469-445X. doi: 10.1113/expphysiol.2009.051961. URL http://www.pubmedcentral.nih.gov/articlerender.fcgi?artid=2995811&tool=pmcentrez&rendertype=abstract. (Cited on pages 1, 2, and 3.)

[41] Longnian Lin, Guifen Chen, Kun Xie, Kimberly a Zaia, Shuqing Zhang, and Joe Z Tsien. Large-scale neural ensemble recording in the brains of freely behaving mice. *Journal of neuroscience methods*, 155(1):28–38, July 2006. ISSN 0165-0270. doi: 10.1016/j.jneumeth.2005.12.032. URL http://www.ncbi.nlm.nih.gov/pubmed/16554093. (Cited on pages 1 and 3.)

[42] Xu Liu and Susumu Tonegawa. Optogenetics 3.0. *Cell*, 141(1):22–4, April 2010. ISSN 1097-4172. doi: 10.1016/j.cell.2010.03.019. URL http://www.ncbi.nlm.nih.gov/pubmed/20371341. (Cited on pages 2 and 3.)

[43] Liqun Luo, Edward M Callaway, and Karel Svoboda. Genetic dissection of neural circuits. *Neuron*, 57(5):634–60, March 2008. ISSN 1097-4199. doi: 10.1016/j.neuron.2008.01.002. URL http://www.pubmedcentral.nih.gov/articlerender.fcgi?artid=2628815&tool=pmcentrez&rendertype=abstract. (Cited on page 3.)

[44] Linda Madisen, Theresa a Zwingman, Susan M Sunkin, Seung Wook Oh, Hatim a Zariwala, Hong Gu, Lydia L Ng, Richard D Palmiter, Michael J Hawrylycz, Allan R Jones, Ed S Lein, and Hongkui Zeng. A robust and high-throughput Cre reporting and characterization system for the whole mouse brain. *Nature neuroscience*, 13(1):133–40, January 2010. ISSN 1546-1726. doi: 10.1038/nn.2467. URL http://www.pubmedcentral.nih.gov/articlerender.fcgi?artid=2840225&tool=pmcentrez&rendertype=abstract. (Cited on page 4.)

[45] Linda Madisen, Tianyi Mao, Henner Koch, Jia-min Zhuo, Antal Berenyi, Shigeyoshi Fujisawa, Yun-Wei a Hsu, Alfredo J Garcia, Xuan Gu, Sebastien Zanella, Jolene Kidney, Hong Gu, Yimei Mao, Bryan M Hooks, Edward S Boyden, György Buzsáki, Jan Marino Ramirez, Allan R Jones, Karel Svoboda, Xue Han, Eric E Turner, and Hongkui Zeng. A toolbox of Cre-dependent optogenetic transgenic mice for light-induced

activation and silencing. *Nature neuroscience*, 15(5):793–802, May 2012. ISSN 1546-1726. doi: 10.1038/nn.3078. URL http://www.pubmedcentral.nih.gov/articlerender.fcgi?artid=3337962&tool=pmcentrez&rendertype=abstract. (Cited on pages 4 and 17.)

[46] Niall McAlinden, David Massoubre, Elliot Richardson, Erdan Gu, Shuzo Sakata, Martin D Dawson, and Keith Mathieson. Thermal and optical characterization of micro-LED probes for in vivo optogenetic neural stimulation. *Optics letters*, 38(6):992–4, March 2013. ISSN 1539-4794. URL http://www.ncbi.nlm.nih.gov/pubmed/23503284. (Cited on page 34.)

[47] Toshio Miyashita, Yu R Shao, Jason Chung, Olivia Pourzia, and Daniel E Feldman. Long-term channelrhodopsin-2 (ChR2) expression can induce abnormal axonal morphology and targeting in cerebral cortex. *Frontiers in neural circuits*, 7(January):8, January 2013. ISSN 1662-5110. doi: 10.3389/fncir.2013.00008. URL http://www.pubmedcentral.nih.gov/articlerender.fcgi?artid=3560348&tool=pmcentrez&rendertype=abstract. (Cited on page 31.)

[48] Dmitry A Molotkov, Alexey Y Yukin, Ramil A Afzalov, and Leonard S Khiroug. Gene delivery to postnatal rat brain by non-ventricular plasmid injection and electroporation. *Journal of visualized experiments : JoVE*, (43), January 2010. ISSN 1940-087X. doi: 10.3791/2244. URL http://www.pubmedcentral.nih.gov/articlerender.fcgi?artid=3157865&tool=pmcentrez&rendertype=abstract. (Cited on page 4.)

[49] G Nagel, T Szellas, S Kateriya, N Adeishvili, P Hegemann, and E Bamberg. Channelrhodopsins: directly light-gated cation channels. *Biochemical Society transactions*, 33(Pt 4):863–6, August 2005. ISSN 0300-5127. doi: 10.1042/BST0330863. URL http://www.ncbi.nlm.nih.gov/pubmed/16042615. (Cited on page 2.)

[50] Georg Nagel, Tanjef Szellas, Wolfram Huhn, Suneel Kateriya, Nona Adeishvili, Peter Berthold, Doris Ollig, Peter Hegemann, and Ernst Bamberg. Channelrhodopsin-2, a directly light-gated cation-selective membrane channel. *Proceedings of the National Academy of Sciences of the United States of America*, 100(24):13940–5, November 2003. ISSN 0027-8424. doi: 10.1073/pnas.1936192100. URL http://www.pubmedcentral.nih.gov/articlerender.fcgi?artid=283525&tool=pmcentrez&rendertype=abstract. (Cited on page 2.)

[51] OSRAM Opto Semiconductors GmbH. PointLED long life Enhanced optical Power LED (ThinGaN) LB P4SG , LT P4SG LB P4SG , LT P4SG, 2009. (Cited on page 23.)

[52] Kristen L Pierce, Richard T Premont, and Robert J Lefkowitz. Seven-transmembrane receptors. *Nature reviews. Molecular cell biology*, 3(9):639–50, September 2002. ISSN 1471-0072. doi: 10.1038/nrm908. URL http://www.ncbi.nlm.nih.gov/pubmed/12209124. (Cited on page 2.)

[53] Matthias Prigge, Franziska Schneider, Satoshi P Tsunoda, Carrie Shilyansky, Jonas Wietek, Karl Deisseroth, and Peter Hegemann. Color-tuned channelrhodopsins for multiwavelength optogenetics. *The Journal of biological chemistry*, 287(38):31804–12, September 2012. ISSN 1083-351X. doi: 10.1074/jbc.M112.391185. URL http://www.ncbi.nlm.nih.gov/pubmed/22843694. (Cited on page 2.)

[54] Joseph Register, Andreas Muller, Justin King, Edwin Weeber, Christopher L. Frewin, and Stephen E. Saddow. Silicon Carbide Waveguides for Optogenetic Neural Stimulation. *MRS Proceedings*, 1433:mrss12–1433–h04–20, May 2012. ISSN 1946-4274. doi: 10.1557/opl.2012.1033. URL http://www.journals.cambridge.org/abstract_S1946427412010330. (Cited on page 34.)

[55] Sébastien Royer, Boris V Zemelman, Mladen Barbic, Attila Losonczy, György Buzsáki, and Jeffrey C Magee. Multi-array silicon probes with integrated optical fibers: light-assisted perturbation and recording of local neural circuits in the behaving animal. *The European journal of neuroscience*, 31(12):2279–91, June 2010. ISSN 1460-9568. doi: 10.1111/j.1460-9568.2010.07250.x. URL http://www.pubmedcentral.nih.gov/articlerender.fcgi?artid=2954764&tool=pmcentrez&rendertype=abstract. (Cited on pages 4, 6, 12, and 28.)

[56] N Schmitzer-Torbert, J Jackson, D Henze, K Harris, and a D Redish. Quantitative measures of cluster quality for use in extracellular recordings. *Neuroscience*, 131(1):1–11, January 2005. ISSN 0306-4522. doi: 10.1016/j.neuroscience.2004.09.066. URL http://www.ncbi.nlm.nih.gov/pubmed/15680687. (Cited on page 20.)

[57] B Schobert and J K Lanyi. Halorhodopsin is a light-driven chloride pump. *The Journal of biological chemistry*, 257(17):10306–13, September 1982. ISSN 0021-9258. URL http://www.ncbi.nlm.nih.gov/pubmed/7107607. (Cited on page 3.)

[58] Dennis R Sparta, Alice M Stamatakis, Jana L Phillips, Nanna Hovelsø, Ruud van Zessen, and Garret D Stuber. Construction of implantable optical fibers for long-term optogenetic manipulation of neural circuits. *Nature protocols*, 7(1):12–23, January

2012. ISSN 1750-2799. doi: 10.1038/nprot.2011.413. URL http://www.ncbi.nlm.nih.gov/pubmed/22157972. (Cited on page 6.)

[59] Eran Stark, Tibor Koos, and György Buzsáki. Diode probes for spatiotemporal optical control of multiple neurons in freely moving animals. *Journal of neurophysiology*, 108(1):349–63, July 2012. ISSN 1522-1598. doi: 10.1152/jn.00153.2012. URL http://www.ncbi.nlm.nih.gov/pubmed/22496529. (Cited on pages vii, 4, 6, 12, and 24.)

[60] A M Thomson and S Radpour. Excitatory Connections Between CA1 Pyramidal Cells Revealed by Spike Triggered Averaging in Slices of Rat Hippocampus are Partially NMDA Receptor Mediated. *The European journal of neuroscience*, 3(6):587–601, January 1991. ISSN 0953-816X. URL http://www.ncbi.nlm.nih.gov/pubmed/12106490. (Cited on page 29.)

[61] Kay M Tye and Karl Deisseroth. Optogenetic investigation of neural circuits underlying brain disease in animal models. *Nature reviews. Neuroscience*, 13(4):251–66, April 2012. ISSN 1471-0048. doi: 10.1038/nrn3171. URL http://www.ncbi.nlm.nih.gov/pubmed/22430017. (Cited on pages 1 and 2.)

[62] Marie Vandecasteele, S M, Sébastien Royer, Mariano Belluscio, Antal Berényi, Kamran Diba, Shigeyoshi Fujisawa, Andres Grosmark, Dun Mao, Kenji Mizuseki, Jagdish Patel, Eran Stark, David Sullivan, Brendon Watson, and György Buzsáki. Large-scale recording of neurons by movable silicon probes in behaving rodents. *Journal of visualized experiments : JoVE*, 0(61):e3568, January 2012. ISSN 1940-087X. doi: 10.3791/3568. URL http://www.ncbi.nlm.nih.gov/pubmed/22415550. (Cited on page 17.)

[63] William Walantus, David Castaneda, Laura Elias, and Arnold Kriegstein. In utero intraventricular injection and electroporation of E15 mouse embryos. *Journal of visualized experiments : JoVE*, (6):239, January 2007. ISSN 1940-087X. doi: 10.3791/239. URL http://www.pubmedcentral.nih.gov/articlerender.fcgi?artid=2557118&tool=pmcentrez&rendertype=abstract. (Cited on page 4.)

[64] Jing Wang, Fabien Wagner, David A Borton, Jiayi Zhang, Ilker Ozden, Rebecca D Burwell, Arto V Nurmikko, Rick van Wagenen, Ilka Diester, and Karl Deisseroth. Integrated device for combined optical neuromodulation and electrical recording for chronic in vivo applications. *Journal of neural engineering*, 9(1):016001, February 2012. ISSN 1741-2552. doi: 10.1088/1741-2560/9/1/016001. URL http://www.ncbi.nlm.nih.gov/pubmed/22156042. (Cited on page 34.)

[65] M J West, L Slomianka, and H J Gundersen. Unbiased stereological estimation of the total number of neurons in thesubdivisions of the rat hippocampus using the optical fractionator. *The Anatomical record*, 231(4):482–97, December 1991. ISSN 0003-276X. doi: 10.1002/ar.1092310411. URL http://www.ncbi.nlm.nih.gov/pubmed/1793176. (Cited on page 24.)

[66] Ilana B Witten, Elizabeth E Steinberg, Soo Yeun Lee, Thomas J Davidson, Kelly a Zalocusky, Matthew Brodsky, Ofer Yizhar, Saemi L Cho, Shiaoching Gong, Charu Ramakrishnan, Garret D Stuber, Kay M Tye, Patricia H Janak, and Karl Deisseroth. Recombinase-driver rat lines: tools, techniques, and optogenetic application to dopamine-mediated reinforcement. *Neuron*, 72(5):721–33, December 2011. ISSN 1097-4199. doi: 10.1016/j.neuron.2011.10.028. URL http://www.pubmedcentral.nih.gov/articlerender.fcgi?artid=3282061&tool=pmcentrez&rendertype=abstract. (Cited on page 4.)

[67] Ofer Yizhar, Lief E. Fenno, Thomas J. Davidson, Murtaza Mogri, and Karl Deisseroth. Optogenetics in Neural Systems. *Neuron*, 71(1):9–34, July 2011. ISSN 08966273. doi: 10.1016/j.neuron.2011.06.004. URL http://linkinghub.elsevier.com/retrieve/pii/S0896627311005046. (Cited on pages 2, 3, and 6.)

[68] Kelly Zalocusky and Karl Deisseroth. Optogenetics in the behaving rat: integration of diverse new technologies in a vital animal model. *Optogenetics*, 1:1–17, January 2013. ISSN 2299-3967. doi: 10.2478/optog-2013-0001. URL http://www.degruyter.com/view/j/optog.2013.1.issue/optog-2013-0001/optog-2013-0001.xml. (Cited on pages 1, 4, and 6.)

[69] Feng Zhang, Li-Ping Wang, Edward S Boyden, and Karl Deisseroth. Channelrhodopsin-2 and optical control of excitable cells. *Nature methods*, 3(10):785–92, October 2006. ISSN 1548-7091. doi: 10.1038/nmeth936. URL http://www.ncbi.nlm.nih.gov/pubmed/16990810. (Cited on page 1.)

[70] Feng Zhang, Li-Ping Wang, Martin Brauner, Jana F Liewald, Kenneth Kay, Natalie Watzke, Phillip G Wood, Ernst Bamberg, Georg Nagel, Alexander Gottschalk, and Karl Deisseroth. Multimodal fast optical interrogation of neural circuitry. *Nature*, 446(7136):633–9, April 2007. ISSN 1476-4687. doi: 10.1038/nature05744. URL http://www.ncbi.nlm.nih.gov/pubmed/17410168. (Cited on pages 2 and 3.)

[71] Feng Zhang, Viviana Gradinaru, Antoine R Adamantidis, Remy Durand, Raag D Airan, Luis de Lecea, and Karl Deisseroth. Op-

togenetic interrogation of neural circuits: technology for probing mammalian brain structures. *Nature protocols*, 5(3):439–56, March 2010. ISSN 1750-2799. doi: 10.1038/nprot.2009.226. URL http://www.ncbi.nlm.nih.gov/pubmed/20203662. (Cited on pages 3 and 4.)

[72] Shengli Zhao, JT Ting, HE Atallah, Li Qiu, and Jie Tan. Cell type-specific channelrhodopsin-2 transgenic mice for optogenetic dissection of neural circuitry function. *Nature . . .* , 8(9), 2011. doi: 10.1038/nMeth.1668. URL http://www.nature.com/nmeth/journal/v8/n9/abs/nmeth.1668.html. (Cited on page 1.)

[73] Xin X Zhou, Hokyung K Chung, Amy J Lam, and Michael Z Lin. Optical control of protein activity by fluorescent protein domains. *Science (New York, N.Y.)*, 338(6108):810–4, November 2012. ISSN 1095-9203. doi: 10.1126/science.1226854. URL http://www.ncbi.nlm.nih.gov/pubmed/23139335. (Cited on page 1.)

DECLARATION

I hereby declare that I have written this thesis independently, unless where clearly stated otherwise. I have used only the sources, the data and the support that I have clearly mentioned. This thesis has not been submitted for conferral of degree elsewhere.

Kuopio, Finland, July 2013

Ronny Eichler